SANDIA REPORT

Structural Evaluation of WIPP Disposal Room Raised to Clay Seam G

Byoung Yoon Park and John F. Holland

Structural Evaluation of WIPP Disposal Room Raised to Clay Seam G

Byoung Yoon Park[1] and John F. Holland[2]
[1]-Performance Assessment & Decision Analysis Department
Sandia National Laboratories
4100 National Parks Highway,
Carlsbad, NM 88220-MS1395
[2]-Solid Mechanics Department
Sandia National Laboratories
P.O. Box 5800
Albuquerque, NM 87185-MS0372

Abstract

An error was discovered in the ALGEBBRA script used to calculate the disturbed rock zone around the disposal room and the shear failure zone in the anhydrite layers in the original version. To correct the error, a memorandum of correction was submitted according to the Waste Isolation Pilot Plant (WIPP) Quality Assurance program. The recommended course of action was to correct the error, to repeat the post-process, and to rewrite Section 7.4, 7.5, 8, and Appendix B in the original report. The sections and appendix revised by the post-process using the corrected ALGEBRA scripts are provided in this revision.

The original report summarizes a series of structural calculations that examine effects of raising the WIPP repository horizon from the original design level upward 2.43 meters. Calculations were then repeated for grid changes appropriate for the new horizon raised to Clay Seam G. Results are presented in three main areas: 1. Disposal room porosity, 2. Disturbed rock zone characteristics, and 3. Anhydrite marker bed failure. No change to the porosity surface for the compliance re-certification application is necessary to account for raising the repository horizon, because the new porosity surface is essentially identical. The disturbed rock zone evolution and devolution are charted in terms of a stress invariant criterion over the regulatory period. This model shows that the propagation of the DRZ into the surrounding rock salt does not penetrate through MB 139 in the case of both the original horizon and the raised room. Damaged salt would be expected to heal in nominally 150 years. The shear failure does not occur in either the upper or lower anhydrite layers at the moment of excavation, but appears above and below the middle of the pillar one day after the excavation. The damaged anhydrite is not expected to heal as the salt in the DRZ is expected to.

ACKNOWLEDGMENTS

CONTENTS

FIGURES

TABLES

ACRONYMS

BRAGFLO	BRine And Gas FLOw (a numerical model)
CCA	Compliance Certification Application
CCDF	Complementary Cumulative Distribution Function
CRA	Compliance Recertification Application
CVS	Concurrent Version System
DOE	U.S. Department of Energy
DRZ	Disturbed Rock Zone
EPA	U.S. Environmental Protection Agency
FEM	Finite Element Method
MB	Marker Bed
M-D	Multi-mechanism Deformation
MSF	Cumulative Shear Failure Variable
NWMP	Nuclear Waste Management Procedure
OS	Operating System
PA	Performance Assessment
QAPD	Quality Assurance Program Document
SNL	Sandia National Laboratories
TRU	Transuranic Waste
WIPP	Waste Isolation Pilot Plant
WTS	Westinghouse TRU Solutions
W/S	Workstation

1 INTRODUCTION

1.1 About This Revision

An error was discovered in the ALGEBBRA script used to calculate the disturbed rock zone (DRZ) around the disposal room and the shear failure zone (SFZ) in the anhydrite layers in the original version [Park and Holland, 2004]. To correct the error, a memorandum of correction [Park and Holland, 2006] was submitted according to the Waste Isolation Pilot Plant (WIPP) Quality Assurance (QA) program. This memorandum describes the error, scopes its potential importance, and provides recommendation for remediation.

The recommended course of action was to correct the error, to repeat the post-process under the Concurrent Version System (CVS) script run control [Park and Kirchner, 2005], and to rewrite Section 7.4, 7.5, 8, and Appendix B in the report for Clay Seam G [Park and Holland, 2004]. The sections and appendix revised by the post-process using the corrected ALGEBRA scripts are provided in this revision. The files related to the correction will be stored in the subdirectory of /data/bypark/clayg/correction/ in the CVS on the workstation ELO at Sandia Carlsbad Program Group. In addition, Section 7. 3, which describes the porosity surface, is revised.

1.2 Objective

This report summarizes the calculations of the structural response of waste-filled disposal rooms, raised 2.43 meters above the level of disposal operations at WIPP. The analysis period is 10,000 years after initial waste emplacement. The calculations of the mechanical creep closure response of a disposal room containing waste but no crushed salt backfill were performed to allow three-dimensional porosity surfaces (Figure 1) to be constructed for WIPP performance assessment (PA) activities. On the basis of the calculations, an assessment was made to determine whether raising the repository 2.43 meters (i.e., so the roof is at an elevation coincident with Clay Seam G) has any significant impact on the conceptual models used in the PA.

1.3 Background

The Department of Energy (DOE) on June 26, 2000 asked permission of the Environmental Protection Agency (EPA) to raise the disposal room 2.43 m above the present level. This change means the roof of a disposal room would coincide with the Clay Seam G horizon and the floor would be separated from the underlying Marker Bed 139 by 3.81 m instead of 1.38 m (the existing design separation in disposal panels 1 and 2). The EPA on August 11, 2000 approved the request and agreed that this mining change will enhance operational safety without significantly affecting the long-term performance of the facility. The EPA on August 6, 2002 sent DOE a letter that stated: *"The conceptual model for the repository should reflect the change to raise the level of excavation to clay seam G. The conceptual change should be appropriately addressed in modeling, if warranted."*

The change in the repository horizon was requested to ease ground control efforts. Fractures surrounding the existing horizon tend to coalesce in an arch, which mimics the shear stress trajectories. These patterns can be seen in the underground today where the roof has been taken down along the length of the East 140 drift. The roof rock of the original horizon tends to de-couple at Clay G, as exhibited by the shear fracture patterns. Underground operations personnel believe that roof support requirements and other ground-control maintenance would be greatly reduced if the roof of the disposal rooms is raised to Clay G. Because this change incorporates a geometry of the WIPP underground that is different from the compliance baseline, as modeled for the Compliance Certification Application (CCA), it is necessary to evaluate the impact of this proposed mining change on performance. For this report, the structural implications of raising the repository horizon were assessed using the calculation procedure described in the AP-093 (Park, 2002).

1.4 Overview of Analyses

This analysis was based on the "Final Disposal Room Structural Response Calculations, SAND97-0795" (Stone, 1997a), which was the referenced baseline report for the CCA. The calculational procedures and data described in SAND97-0795 were used in this current analysis so a direct comparison between the results of this analysis and those presented in SAND97-0795 could be made. Therefore, the initial calculations replicated room pressure and porosity histories for various gas generation rates for a period of 10,000 years following excavation and waste emplacement. The data used in this analysis such as the stratigraphy, waste characterization, gas generation potential and material response, etc. are identical to that used in Stone's analysis (Stone, 1997a).

The analysis results are split into three parts. The first one is the change of the porosities due to the disposal room creep closure. The second one is the change of the disturbed rock zone (DRZ) with time. The third one is the change of the shear failure zone in anhydrite with time. The results of the porosity changes will be provided to the BRAGFLO analyst as the look-up table. The results of the DRZ changes provide basic data for performance assessment treatment of the DRZ and the groundwater flow analysis. Results from the anhydrite shear failure provide a structural assessment of marker bed damage that can persist and thereby provide preferred flow paths out of the repository.

The quasistatic, large deformation finite element code SANTOS (Stone, 1997b) version 2.1.7, installed on the Warthog workstation with the Linux operating system, was used for the analyses. SANTOS 2.1.7 was qualified though 21 test cases which are consistent with SANTOS – Verification and Qualification Document of 1996, the validation of SANTOS 2.1.0 (Arguello et al. 1996). The Verification and Validation Plan/Validation Document for SANTOS 2.1.7 discusses the testing in detail (WIPP PA 2003). Figure 2 shows a models and data flow diagram of the WIPP CRA PA calculation. Several processes are performed to generate the CCDF curves. The final goal of the analyses is to produce CCDF curves to compare releases from the repository. The SANTOS results feed BRAGFLO analyses which simulates the brine and gas flow in Salado formation.

1.5 Report Organization

The next section of the report presents the analysis models used in Stone's (1997a) analysis including the disposal room model that describes the disposal room and the waste contents and the geomechanical model that describes, among other features, the idealized stratigraphy. Also included in Section 2 are descriptions of the constitutive models used in the analyses. References for the sources of all of the dimensions, values for constitutive model parameters, and other input information are given in Butcher (1997). Section 3 presents the discretized finite-element model developed to simulate the 2.43 m change in the disposal room elevation. In Section 4, the applied formulation to calculate the change of the DRZ boundary with time is described. Section 5 describes the computer code, SANTOS, used for the analyses. The analyses procedure is described in Section 6. Section 7 describes the results including a comparison of current results with those of Stone (1997a), the disposal room creep closure, the three-dimensional porosity surface, the changes in the DRZ, and the failure pattern in anhydrite. Section 8 provides the summary and conclusions of the analyses.
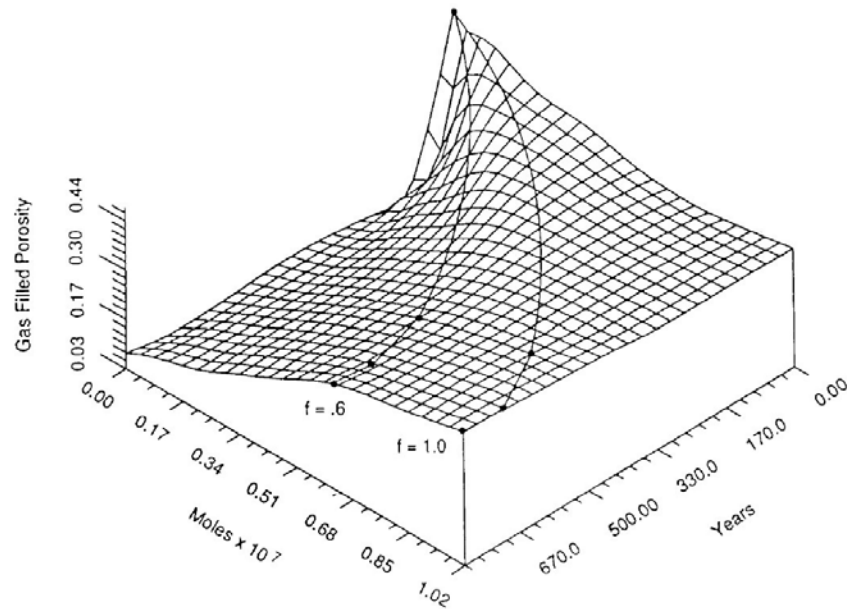
Figure 1: A typical porosity surface used for the 1992 comparison of predicted WIPP performance with 40 CFR Part 191, Subpart B (Butcher and Mendenhall, 1993)

13
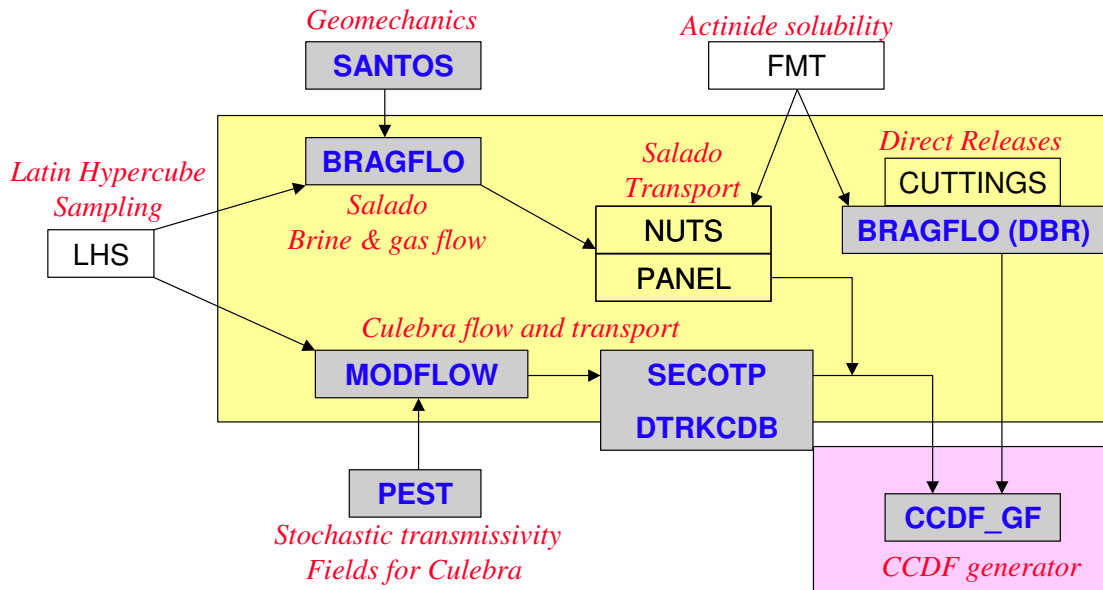
Figure 2: A model and data flow diagram for the WIPP CRA PA.

2 ANALYSIS MODEL

2.1 Disposal Rooms Model

The rectangular-shaped underground disposal rooms are mined at a depth of 655 m from the bedded salt formations in southeastern New Mexico and are designed to dispose of transuranic waste. The regulatory period is 10,000 years. With time, the creep of the rock salt closes the room and encapsulates the waste until equilibrium is established.

2.1.1 Initial porosity

The disposal room model is developed around a rectangular room 3.96 m high by 10.06 m wide by 91.44 m in length with an initial room free volume of 3,644 m^3. The current disposal configuration calls for 6,804 drums of uniformly-distributed unprocessed waste to be stored in the disposal room in 7-pack units. There are 972 of these units stacked three high along the disposal room floor. This analysis considered a disposal room containing wastes only; no crushed-salt and MgO backfill is placed either around the waste or in the void space between drums. The corresponding volume occupied by the waste and the drums is 1,728 m^3.

The transuranic waste form is a combination of metallics, sorbents, cellulose, rubber and plastics, and sludges. Table 1 summarizes the data used in the CCA for characterizing the waste. The initial waste density, ρ_0, is 559.5 kg/m^3 and the solid waste density, ρ_s, is 1,757 kg/ m^3. The initial waste density is the sum of the densities of the constituent waste forms. Using the following definition of porosity, $\phi = 1 - \rho_0 / \rho_s$ (refer to App. A-1)), the initial waste porosity, ϕ_0, is calculated to be 0.681 resulting in an initial solid volume of 551.2 m^3. Using the difference of the undeformed disposal room volume and the initial solid volume to calculate the total void volume of the room, the initial porosity of the undeformed disposal room is determined to be 0.849 (refer to App. A-2).

Table 1: WIPP CH-TRU Waste Material Parameter Disposal Inventory (Butcher, 1997)

Waste Form	Waste Density (kg/m^3)	Volume Fraction
Metallic	122.	0.218
Sorbents	40.	0.071
Cellulose	170.	0.304
Rubber & Plastics	84.	0.150
Sludges	143.5	0.256
Sum	*559.5*	*0.999*

2.1.2 Gas generation potential

The gas generation potential and gas production rate corresponding to the reference case are derived from two sources: anoxic corrosion and microbial activity. Butcher (1997) reports that the estimated gas production potential from anoxic corrosion will be 1,050 *moles/drum* with a production rate of 1 *mole/drum/year*. The gas production potential from microbial activity is estimated to be 550 *moles/drum* with a production rate of 1 *mole/drum/year*. Based on these potentials and production rates, microbial activity ceases at 550 years, while anoxic corrosion will continue until 1,050 years after emplacement. The total amount of gas generated in a disposal room for the reference case was based on 6,804 unprocessed waste drums per room. The total gas potential for the reference case is shown in Figure 3. The gas generation potential assumes that no gas bleeds off through flow through the surrounding lithologies.

The gas pressure in the disposal room was computed from the ideal gas law based on the current free volume in the room. Specifically, the gas pressure, p_g, was computed with the following relationship:

$$p_g = f \cdot \frac{NRT}{V} \tag{1}$$

where N, R and T are the mass of gas in g-moles for the baseline case, the universal gas constant, and the absolute temperature in degrees Kelvin, respectively. For the current analyses, the absolute temperature is taken to be 300 °K. The variable, V, is the current free volume of the room. For each iteration in the analysis, the current room volume is calculated based on the displaced positions of the nodes on the boundary of the room. The free room volume, V, is computed by subtracting the solid volume of the waste, 551.2 m^3, from the current room volume. The gas generation variable, f, is a multiplier used in the analyses to scale the pressure by varying the amount of gas generation. A value of f=1 corresponds to an analysis incorporating full gas generation, while a value of f=0 corresponds to an analysis incorporating no internal pressure increase due to gas generation. This portion of the analysis is identical to that implemented by Stone (1997a).

The porosity surface defines the relationship between disposal room porosity, amount of gas present in that porosity, and time. The porosity can be computed directly from the disposal room deformed shape. The concept of the porosity surface comes from the observation that the disposal room closure is directly influenced by gas generation. This observation allows a surface to be constructed incorporating the closure results for various values of f, which is a convenient way to express the amount of gas generation occurring.
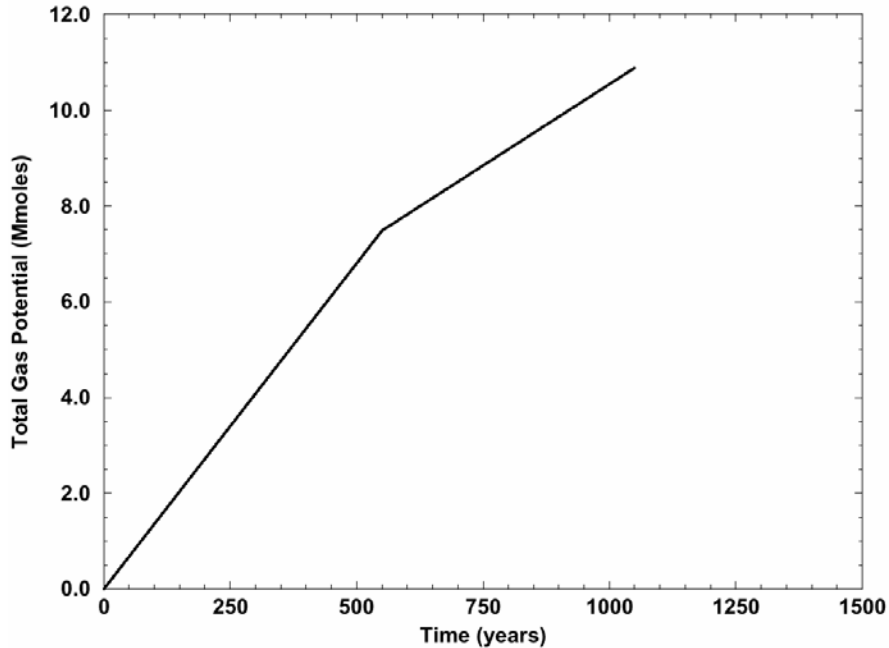
Figure 3: History of the reference gas generation potential used for the disposal room analyses, *f* = 1.0. (Stone, 1997a)

2.2 Geomechanical Model

2.2.1 Stratigraphy

The base idealized stratigraphy for the WIPP underground used in the geomechanical model is the stratigraphy as defined by Munson et al. (1989). This stratigraphy is shown in Figure 4 with the disposal room located at the original horizon. Work by Osnes and Labreche, included as an appendix in Butcher (1997), quantified the differences in room closure obtained by assuming different stratigraphic models that incorporate different numbers of clay seams and anhydrite marker beds. They compared a full stratigraphic model consisting of 12 clay seams and 7 anhydrite layers to analysis results using smaller combinations of clay seams and marker beds. Their work showed that room closure and room porosity results from the full model could be reproduced using the simpler models. Butcher (1997) performed a set of calculations that identified a simple stratigraphic model that captured most of the room closure and room porosity results seen in the more complex stratigraphic models. The stratigraphic model used in Stone's (1997a) analyses is composed of mainly argillaceous salt with a clean salt layer above the disposal room between Clay G and Clay I, anhydrite MB 139, and a thin anhydrite layer located in the clean salt layer identified as anhydrite A. Based on the prior study by Butcher (1997), no clay seams were included in the model. The final stratigraphic model used for Stone's (1997a) analyses is shown in Figure 5.

This stratigraphic model is changed as shown in Figure 6 to raise the disposal room by 2.43 m. The stratigraphic model, including disposal room dimensions, is identical to the previous model, except the disposal room is translated vertically to make the room ceiling coincident with Clay Seam G.

17

DEPTH WITH RESPECT
TO REFERENCE
STRATIGRAPHY ZERO (m)
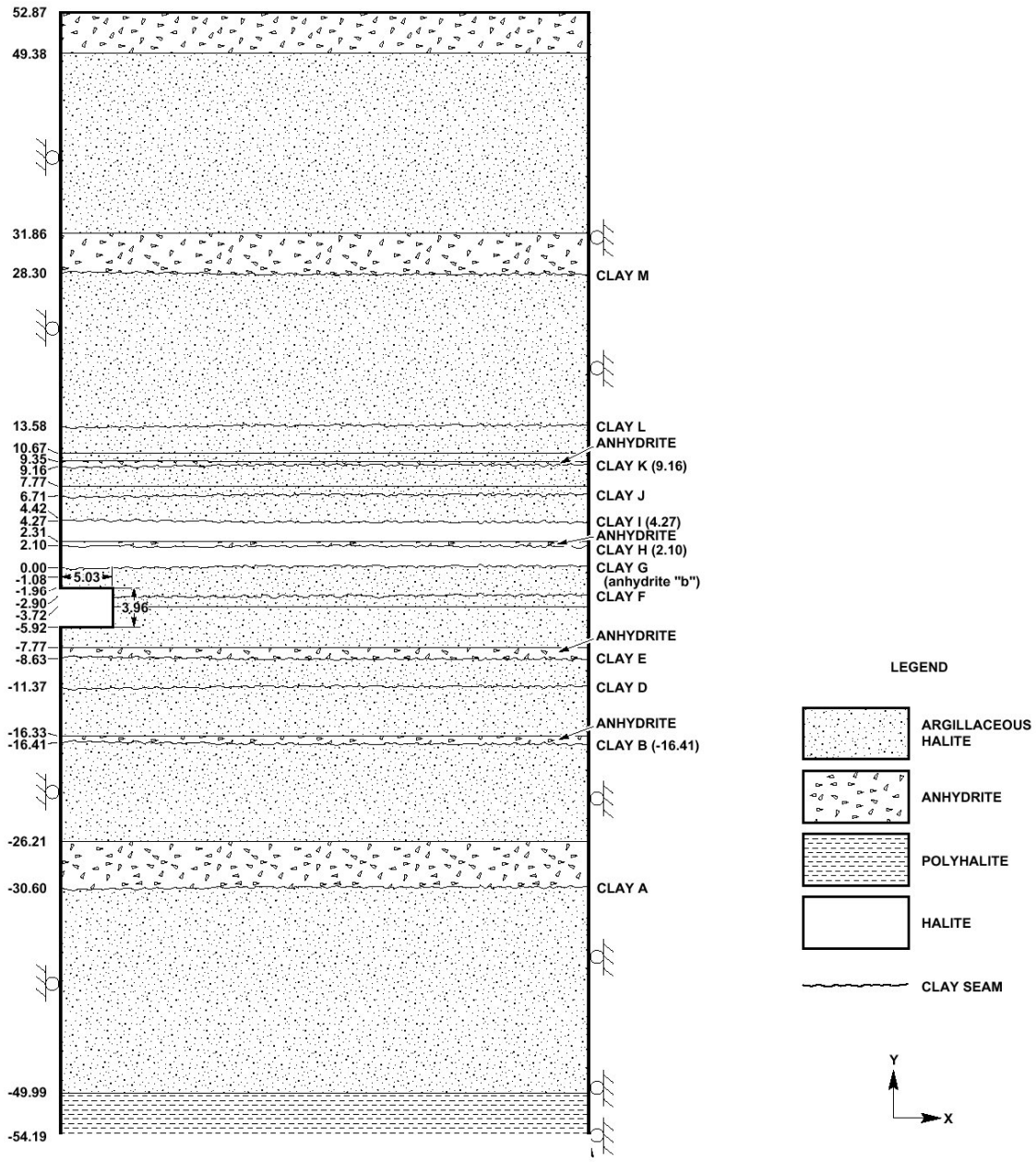
Figure 4: Idealized stratigraphy near the disposal room horizon defined by
Munson et al. (1989)

18

DEPTH WITH RESPECT
TO REFERENCE
STRATIGRAPHY ZERO (m)   13.57 MPa

52.87

ANHYDRITE

CLAY G

4.27
2.31
2.10
0.00
-2.43
5.03
3.96
-6.39   MB139
-7.77   ANHYDRITE
-8.63

LEGEND

ARGILLACEOUS
HALITE

ANHYDRITE

HALITE

Y
X

ALL DIMENSIONS IN METERS
g = 9.79 m/s^2
ρ = 2.30 Mg/m^3

-54.19

20.27 m

T/Q-13012-1-16075
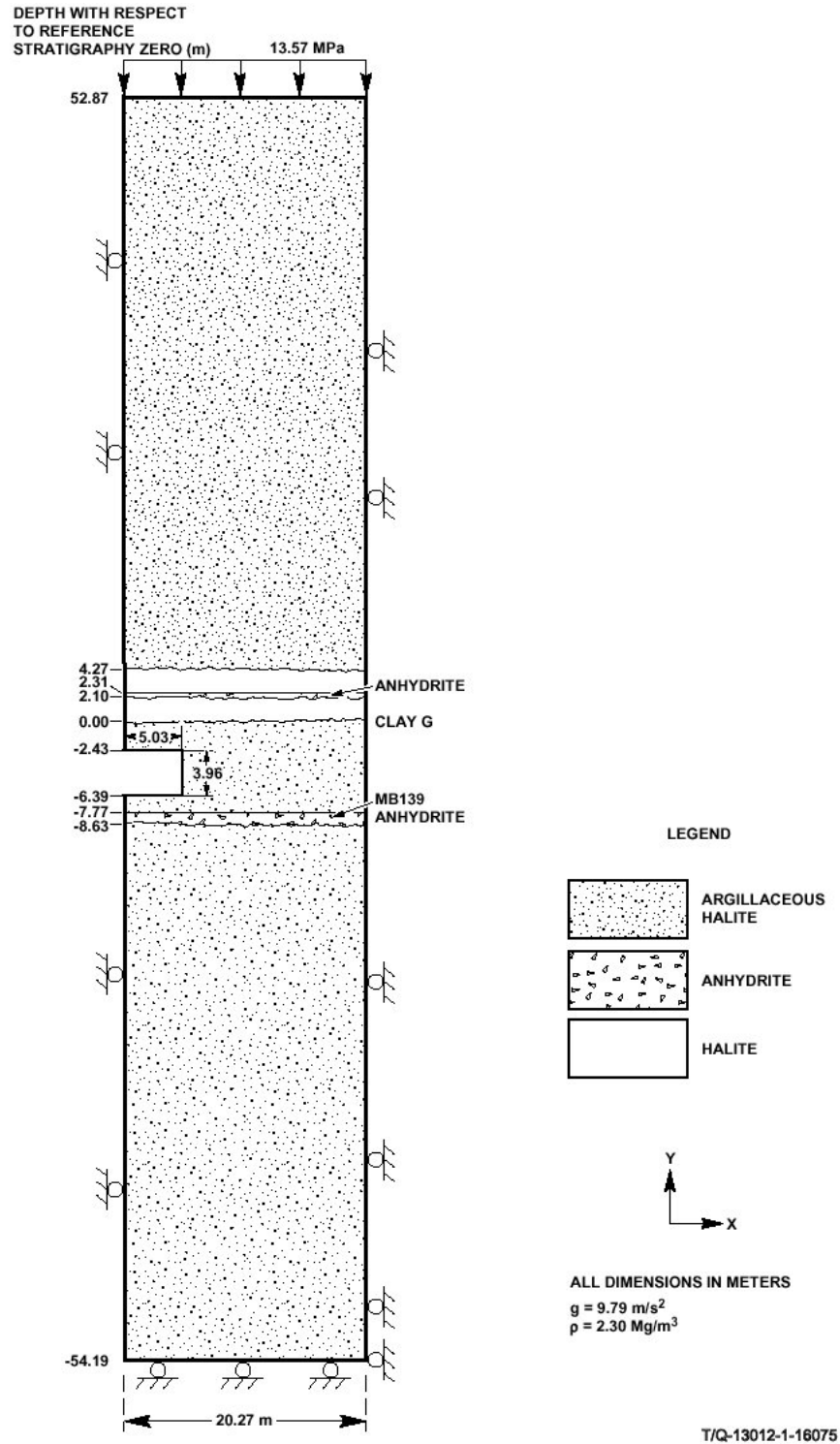
Figure 5: Simplified stratigraphic model for the current level of the disposal room (Butcher, 1997)

19
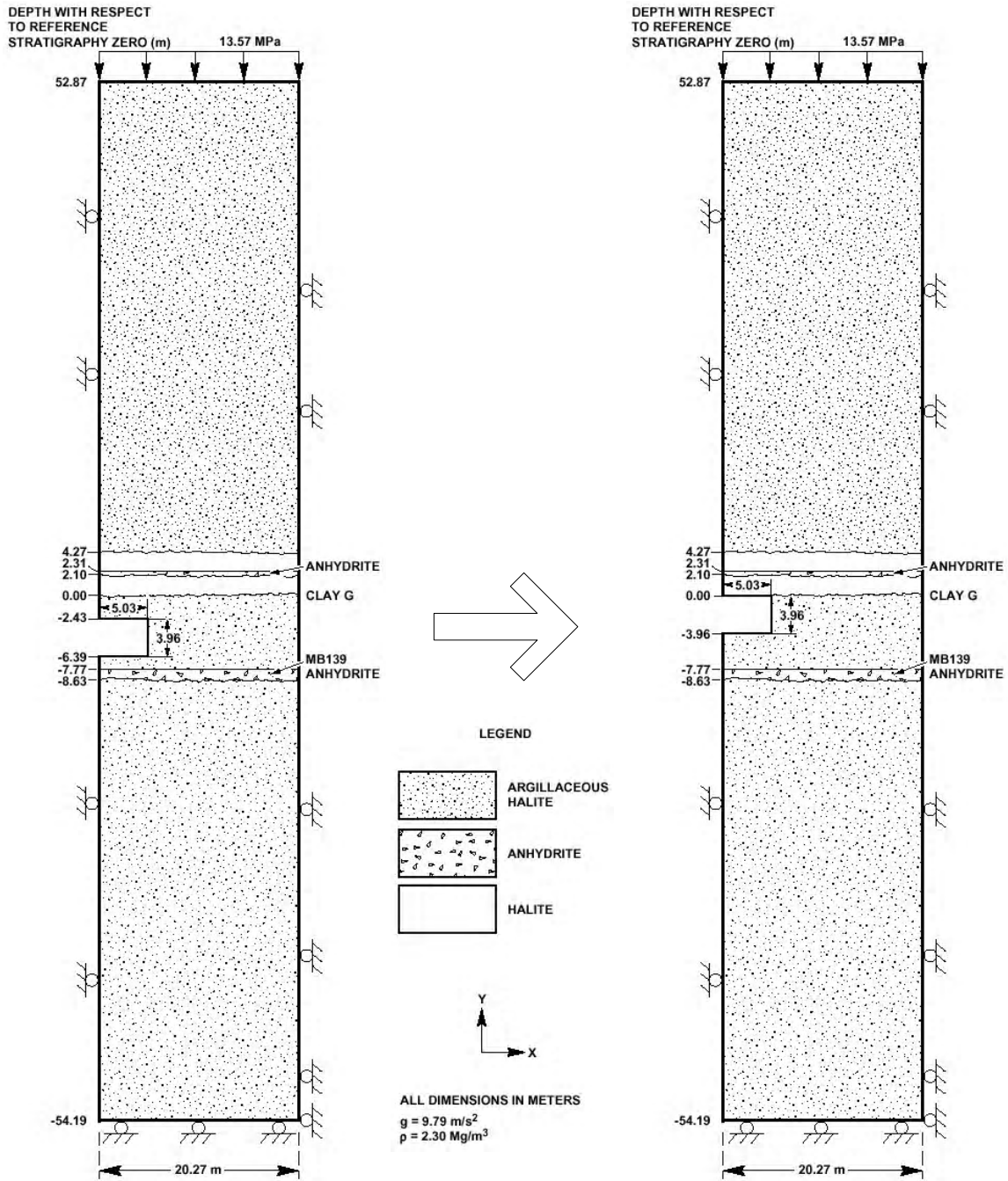
Figure 6: Simplified stratigraphic model used for Stone's (1997a) analyses (left) and the new one (right).

20

2.2.2 Halite constitutive model

A multi-mechanism deformation (M-D) model proposed by Munson and Dawson (1979, 1982, 1984) and extended by Munson et al. (1989), has been included in SANTOS to model the creep behavior of rock salt. This model was used for the clean and argillaceous salt. The model can be decomposed into (1) an elastic volumetric part defined by

$$\varepsilon_{kk} = \frac{\sigma_{kk}}{3K} \tag{2}$$

where, ε_{ij} = the total strain components

σ_{ij} = the total stress components

K = the elastic bulk modulus

and (2) a deviatoric part defined by

$$\dot{s}_{ij} = 2G\left(\dot{e}_{ij} - F\dot{\varepsilon}_s \left[\frac{s_{ij}\cos 2\theta}{\sqrt{J_2}\cos 3\theta} + \frac{\sqrt{3}\sin\theta}{J_2\cos 3\theta}\left\{ s_{ip}s_{pj} - \frac{2}{3}J_2\delta_{ij} \right\} \right] \right) \tag{3}$$

where, $s_{ij} = \sigma_{ij} - \dfrac{\sigma_{kk}}{3}$: the deviatoric stress

G = the elastic shear modulus

$e_{ij} = \varepsilon_{ij} - \dfrac{\varepsilon_{kk}}{3}$: the deviatoric strain

δ_{ij} = Kronecker delta = 1 for i = j; = 0 for i ≠ j

J_2 and   are the second invariant of the deviator stress and the Lode angle, respectively, and are defined later.

The second term of the above equation represents the creep contribution. In the creep term of Equation 3, F is a multiplier on the steady-state creep rate to simulate the transient creep response according to the following equation,

$$F = \begin{cases} e^{\Delta[1-\zeta/\varepsilon_t^*]^2}, & \zeta < \varepsilon_t^* \\ 1 & \zeta = \varepsilon_t^* \\ e^{-\delta[1-\zeta/\varepsilon_t^*]^2} & \zeta > \varepsilon_t^* \end{cases} \tag{4}$$

where, Δ = work-hardening parameter

δ = recovery parameter

ε_t^* = so-called transient strain limit

Finally, ζ is an internal state variable whose rate of change is determined by the following evolutionary equation,

$$\dot{\zeta} = (F - 1)\dot{\varepsilon}_s \tag{5}$$

In Equation 4, the work-hardening parameter Δ is defined as,

$$\Delta = \alpha + \beta \log(\overline{\sigma}/G) \tag{6}$$

where, α and β are constants. The variable $\overline{\sigma}$ is the equivalent Tresca stress given by

$$\overline{\sigma} = 2\sqrt{J_2}\cos\theta \tag{7}$$

where, $\theta = \dfrac{1}{3}\arcsin\left[\dfrac{-3\sqrt{3}J_3}{2(J_2)^{3/2}}\right]$ is the Lode angle limited to the range: $(-\dfrac{\pi}{6} \le \theta \le \dfrac{\pi}{6})$.

$J_2 = \dfrac{1}{2}s_{pq}s_{qp}$: second invariant of the stress deviator

$J_3 = \dfrac{1}{3}s_{pq}s_{qr}s_{rp}$: third invariant of the stress deviator

The recovery parameter, δ, is held constant. The transient strain limit is given by

$$\varepsilon_t^* = K_0 e^{cT}(\overline{\sigma}/G)^M \tag{8}$$

where K_0, c, and M are constants.

The steady-state, or secondary creep strain rate, $\dot{\varepsilon}_s$, is given by

$$\dot{\varepsilon}_s = A_1 e^{-Q_1/RT}\left(\frac{\overline{\sigma}}{G}\right)^{n_1} + A_2 e^{-Q_2/RT}\left(\frac{\overline{\sigma}}{G}\right)^{n_2} + |H|\left[B_1 e^{-Q_1/RT} + B_2 e^{-Q_2/RT}\right]\sinh\left[\frac{q(\overline{\sigma} - \sigma_{0)}}{G}\right] \tag{9}$$

where the A_i s and B_i s are constant

    Q_i s are activation energies
    T = the absolute temperature
    R = the universal gas constant
    n_i s are the stress exponents
    q = the so-called stress constant
    σ_0= the stress limit of the dislocation slip mechanism
    $|H|$ = the Heaviside step function with the argument $(\overline{\sigma} - \sigma_0)$

The material constants corresponding to the clean and argillaceous salt, used in the analyses, are given in Table 2 and Table 3.

Table 2: Salt elastic properties (Butcher, 1997)

G (MPa)	E (MPa)	ν
12,400	31,000	0.25

Table 3: Salt creep properties (Munson et al., 1989)

Parameters (Units)	Clean Salt	Argillaceous Salt
A_1 (/sec)	8.386E22	1.407E23
Q_1 (cal/mole)	25,000	25,000
n_1	5.5	5.5
B_1 (/sec)	6.086E6	8.998E6
A_2 (/sec)	9.672E12	1.314E13
Q_2 (cal/mole)	10,000	10,000
n_2	5.0	5.0
B_2 (/sec)	3.034E-2	4.289E-2
σ_0 (MPa)	20.57	20.57
Q	5,335	5,335
M	3.0	3.0
K_0	6.275E5	2.470E6
c (/T)	9.198E-3	9.198E-3
α	-17.37	-14.96
β	-7.738	-7.738
δ	0.58	0.58

2.2.3 Waste constitutive model

The stress-strain behavior of the waste was represented by a volumetric plasticity model (Stone, 1997b) with a piecewise linear function defining the relationship between the mean stress and the volumetric strain. Compaction experiments on simulated waste were used to develop this relationship. The deviatoric response of the waste material has not been characterized. It is anticipated that when a drum filled with loosely compacted waste is compressed axially, the drum will not undergo significant lateral expansion until most of the void space inside the drum has been eliminated (Stone, 1996).

For the volumetric plasticity model, the yield surface in the principal stress space is a surface of revolution with its axis centered about the hydrostat and the open end pointing into the compression direction (Figure 7). The open end is capped with a plane that is at right angles to the hydrostat. The deviatoric part is elastic-perfectly plastic so the surface of revolution is stationary in stress space. The volumetric part has variable strain hardening so the end plane moves outward during volumetric yielding. The volumetric hardening is defined by a set of pressure-volumetric strain relations. A flow rule is used such that deviatoric strains produce no volume change (associated flow). The model is best broken into volumetric and deviatoric parts with the deviatoric part resembling conventional plasticity. The volumetric yield function is a product of two functions, ϕ_s and ϕ_p, describing the surface of revolution and the plane normal to the pressure axis, respectively. These are given by

$$\phi_s = \frac{1}{2} s_{ij} s_{ij} - a_0 + a_1 p + a_2 p^2 \tag{10}$$

$$\phi_p = p - g(\varepsilon_v) \tag{11}$$

where a_0, a_1, a_2 are constants defining the deviatoric yield surface, p is the pressure, and ε_v is the volumetric strain. The form of g is defined in this problem by a set of piecewise linear segments relating to pressure-volumetric strain. Table 4 lists the pressure-volumetric strain data used for the waste drum model and the data are plotted in Figure 8. Note that the final point listed in the table is a linear extrapolation beyond the curve data given in Butcher (1997). The final pressure of 12 MPa corresponds to an axial stress on a waste drum of 36 MPa. The elastic material parameters and constants defining the yield surface are given in Table 5.
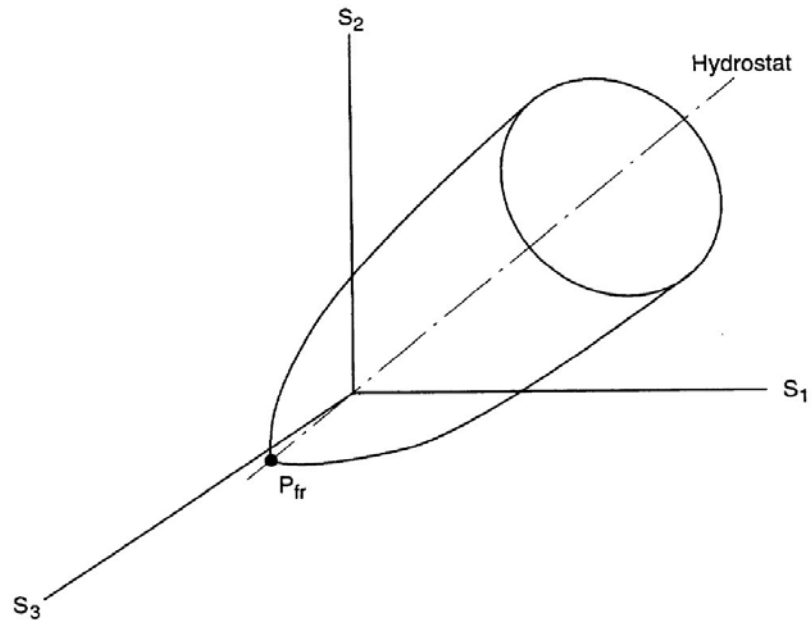
TRI-6348-13-0

Figure 7: Pressure-dependent yield surface for the waste material model (Stone, 1997b)
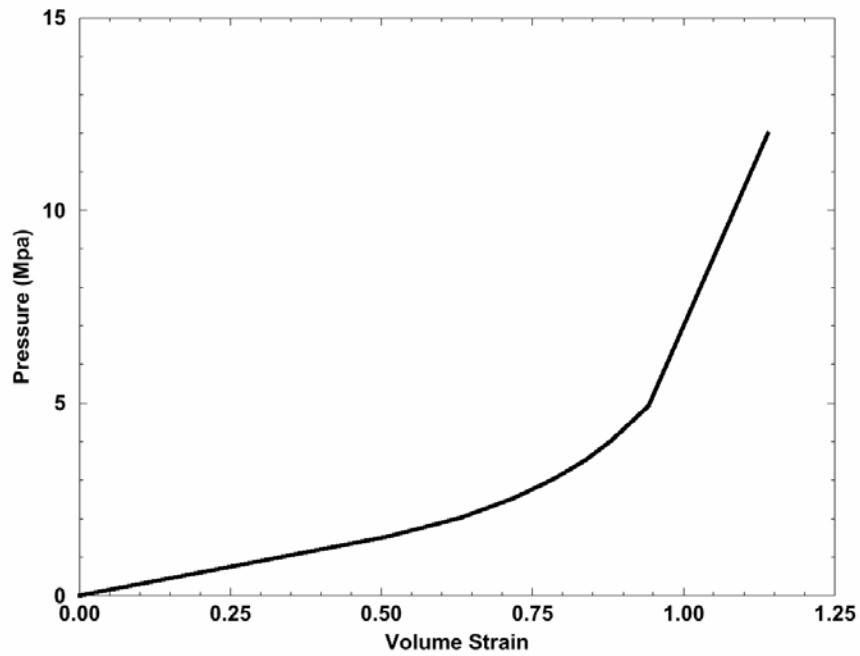
Figure 8: Curve of the pressure-bulk strain input to the volumetric plasticity model used to model the waste drums (Stone, 1997a)

25

Table 4: Pressure-volumetric strain data used in the volumetric-plasticity model for the waste drums (Butcher, 1997)

Pressure (MPa)	$\ln(\rho/\rho_0)$
1.53	0.510
2.03	0.631
2.53	0.719
3.03	0.786
3.53	0.838
4.03	0.881
4.93	0.942
12.0	1.14

Table 5: Material constants used with the volumetric plasticity model for the waste (Butcher, 1997)

Parameter	Value
G	333.0 MPa
K	222.0 MPa
a_0	1.0 MPa
a_1	3.0
a_2	0.

2.2.4 Anhydrite constitutive model

The anhydrite layer beneath the disposal room is expected to experience inelastic material behavior. The MB 139 anhydrite layer is considered isotropic and elastic until yield occurs (Butcher, 1997). Once the yield stress is reached, plastic strain begins to accumulate. Yield is assumed to be governed by the Drucker-Prager criterion

$$\sqrt{J_2} = C - aI_1 \tag{12}$$

where J_2 = the second deviatoric stress invariant
    I_1 = the first stress invariant (σ_{kk})

A nonassociative flow rule is used to determine the plastic strain components. The elastic properties and Drucker-Prager constants, C and a, for the anhydrite are given in Table 6. To calculate the shear failure region in anhydrite, the ALGEBRA file to represent Equation 12 is provided in Appendix B.

Table 6: Elastic and Drucker-Prager constants for anhydrite (Butcher, 1997)

Material	Young's Modulus (GPa)	Poisson's Ratio	C (MPa)	a
Anhydrite	75.1	0.35	1.35	0.45

The input to the soil and crushable foam model in the SANTOS code requires the analyst to provide TWO MU, (2μ), and the BULK MODULUS, K. The conversion from Young's modulus, E, and Poisson's ratio, ν, to the SANTOS input parameters is given from the following relationships taken from Fung (1965):

$$2\mu = \frac{E}{(1+\nu)} \tag{13}$$

$$K = \frac{E}{3(1-2\nu)} \tag{14}$$

SANTOS requires the input to the material model which describes the anhydrite nonlinear response to be given in terms of effective stress, $\bar{\sigma} = \sqrt{3J_2}$, and pressure, $p = \frac{I_1}{3}$. Rewriting Equation 12 in terms of $\bar{\sigma}$ and p, the following relationship is obtained:

$$\bar{\sigma} = \sqrt{3}C - 3\sqrt{3}ap \tag{15}$$

The SANTOS input constant A_0 is $\sqrt{3}C$ and the input constant A_1 is $3\sqrt{3}a$. The set of SANTOS input parameters for the anhydrite is given in Table 7.

Table 7: SANTOS input parameters for the anhydrite layers

Material	TWO MU (GPa)	BULK MODULUS (GPa)	A_0 (MPa)	A_1	A_2
Anhydrite	55.6	83.4	2.3	2.338	0.0

The calculation sheet to compute the SANTOS input parameters using the above data is provided in Appendix A-3.

3 MESH GENERATION

A two-dimensional plane strain disposal room model that was converted from the simplified stratigraphy (Figure 6, right), as shown in Figure 9, is used for the SANTOS analyses. This discretized finite element model is changed from Stone's (1997a) mesh, as shown in Figure 10, to raise the disposal room by 2.43 m. The mesh is changed as little as possible to minimize the margin of error resulting from the change. The mesh, excluding the elements immediately adjacent to the room, is the same as the one made by Stone (1997a).

The discretized model represents the room as one of an infinite number of rooms located at the repository horizon. Making use of symmetry, only half of the room is modeled. The left and right boundaries are planes of symmetry. The upper and lower boundaries are located approximately 50 m from the room. A lithostatic stress ($\sigma_x = \sigma_y = \sigma_z$) that varies with depth is used as the initial stress on the configuration and the gravity forces are included. The model contains 1,680 quadrilateral uniform-strain elements and 1,805 nodal points. A zero-displacement boundary condition in the horizontal direction ($U_x = 0.0$) was applied on both the left and right boundaries of the model to represent the symmetry condition of a half-symmetry disposal room in an infinite array of rooms. A prescribed normal traction of 13.57 MPa was applied on the upper boundary and a vertical zero-displacement boundary condition ($U_y = 0.0$) was applied on the lower boundary to react to the overburden load. An adaptive internal pressure, p_g, was applied around the boundary of the disposal room.

The basic half-symmetry disposal room dimensions are 3.96 m high by 5.03 m wide with a significant portion of this area containing the stored CH-TRU waste. The waste is stored in 7-packs stacked three high along the drift with a height of 2.676 m. This storage configuration contains a large amount of void volume associated with each 7-pack (Figure 11). To obtain the waste volume dimensions used in the calculations, the assumption is made that each waste drum will laterally deform independent of one another. The void space between drums must be eliminated in order to have an accurate continuum representation of the waste response. To eliminate the void space between drums, the assumption is made that the lateral deformation of a configuration of drums caused by the inward movement of the walls of the disposal room is sufficient to eliminate space between the drums early in the closure process at low stress levels. In other words, the lateral deformation of the disposal room rib compresses the 7-packs causing the void space between the drums to be removed with little or no resistance by the waste drums themselves. This assumption allows calculation of an effective lateral dimension for the waste after lateral collapse of the space between the drums is complete. The lateral dimension of the waste drums within the disposal room is determined from the total initial waste volume of 1,728 m^3. Equation 16 was used to determine the compressed dimensions of the waste used for the continuum representation.

$$(W_0 - 2D)(L_0 - 2D)H_0 = 1728 \qquad (16)$$

where, W_0 = the nominal uncompressed width of the stored waste in the disposal room
(8.6 m)

L_0 = the nominal length of the disposal room available for storing waste (89.1 m)

H_0 = the height of the three stacked waste containers (2.676 m)

D = the amount of space that must be eliminated between the drums

Note in Equation 16 that the length of the disposal room has been modified by the same amount, D. Solving for D, we find that the modified width of the waste is 7.35 m and the modified length is 87.85 m (refer to App. A-4).

Contact surfaces were defined between the waste and room boundaries to model the contact and sliding that occurs as the room deforms and entombs the waste. Specifically, contact surfaces were defined between the waste and floor of the room, the waste and room rib, and the waste and ceiling. All of the contact surfaces were allowed to separate if the forces between the surfaces reached a tensile value. This feature allows the room to reopen due to gas generation within the disposal room.
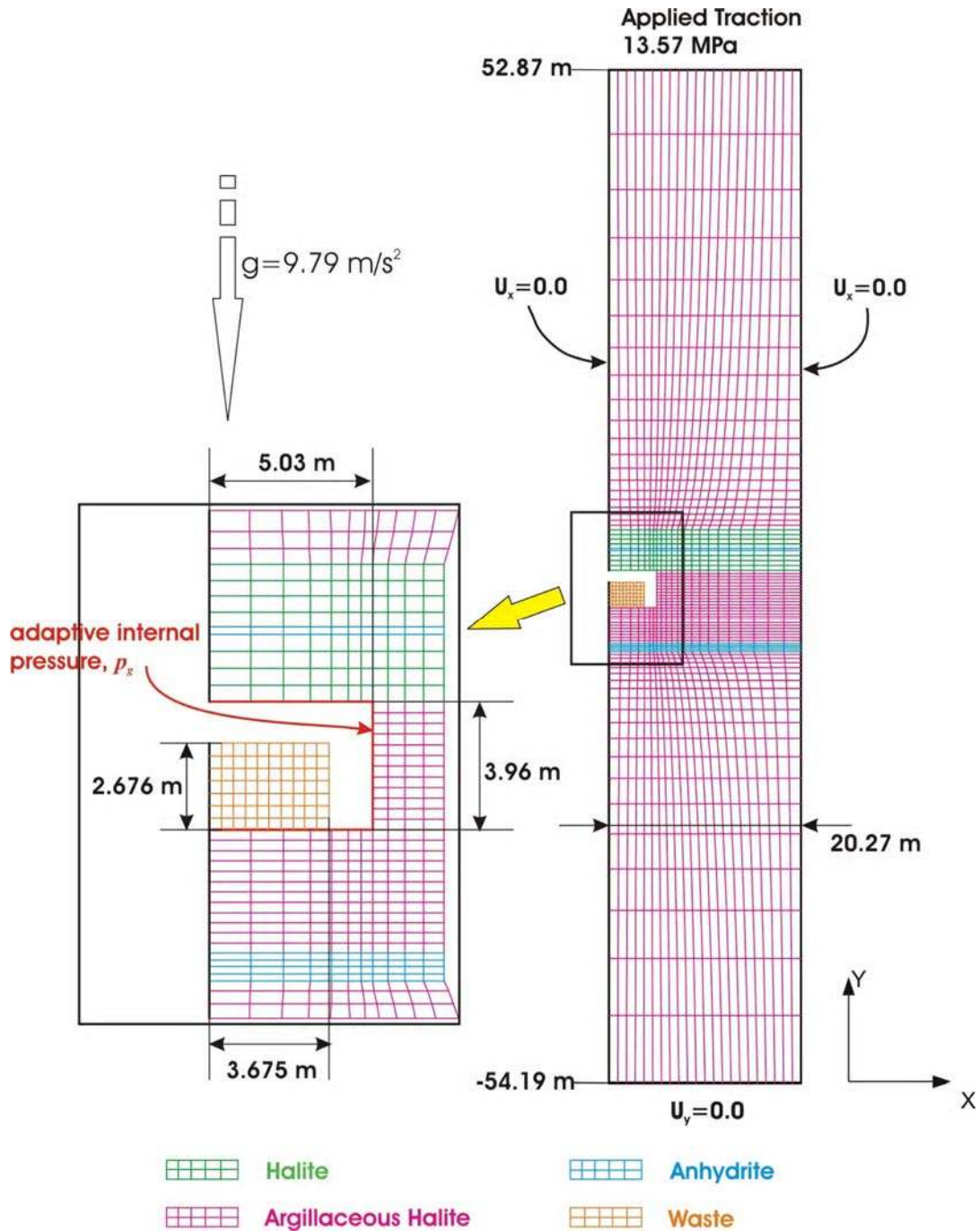
Figure 9: Mesh discretization and boundary conditions used for the SANTOS analyses
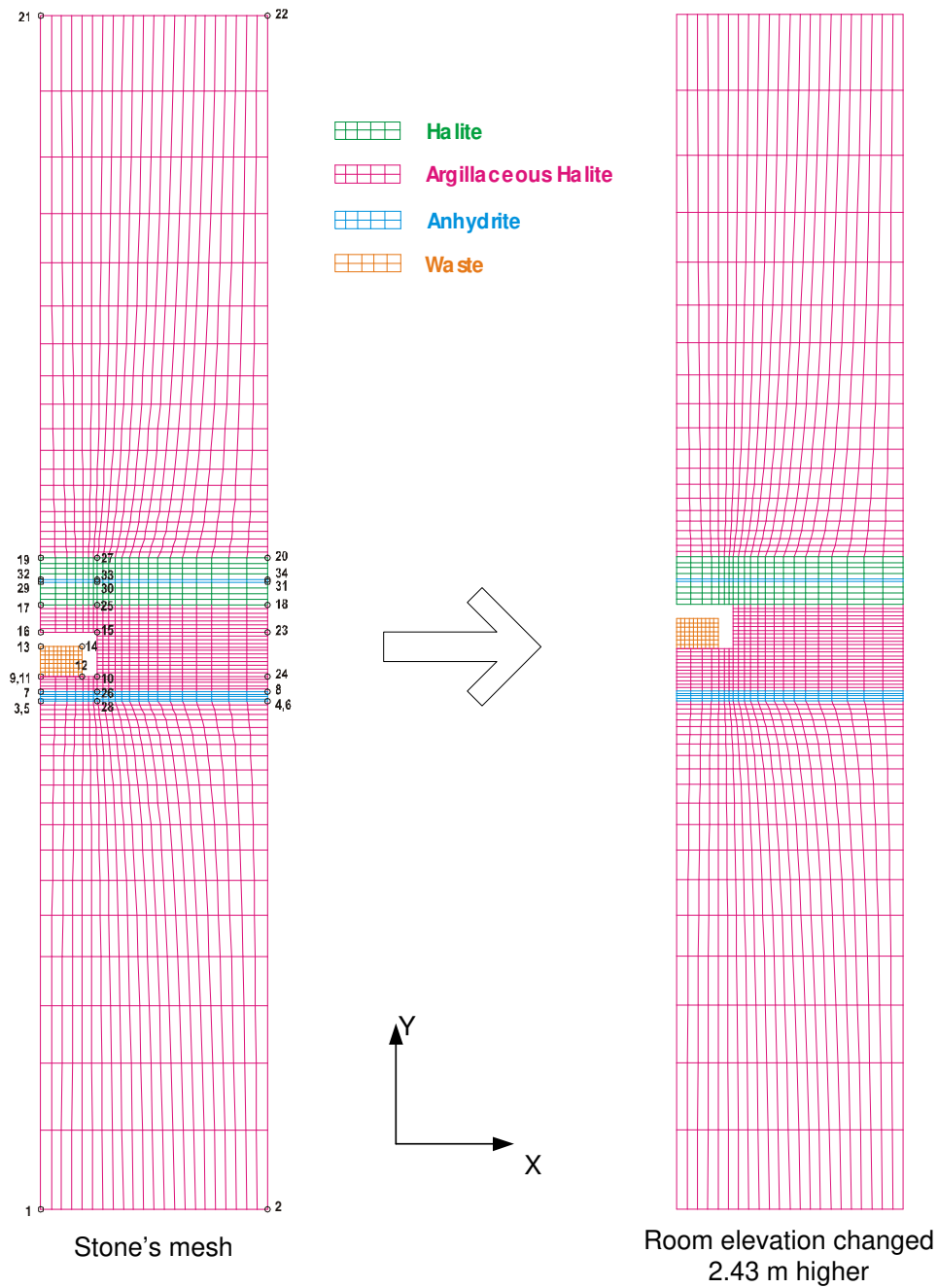
Figure 10: The discretized finite element model is changed from Stone's (1997a) mesh to raise the disposal room by 2.43 m.
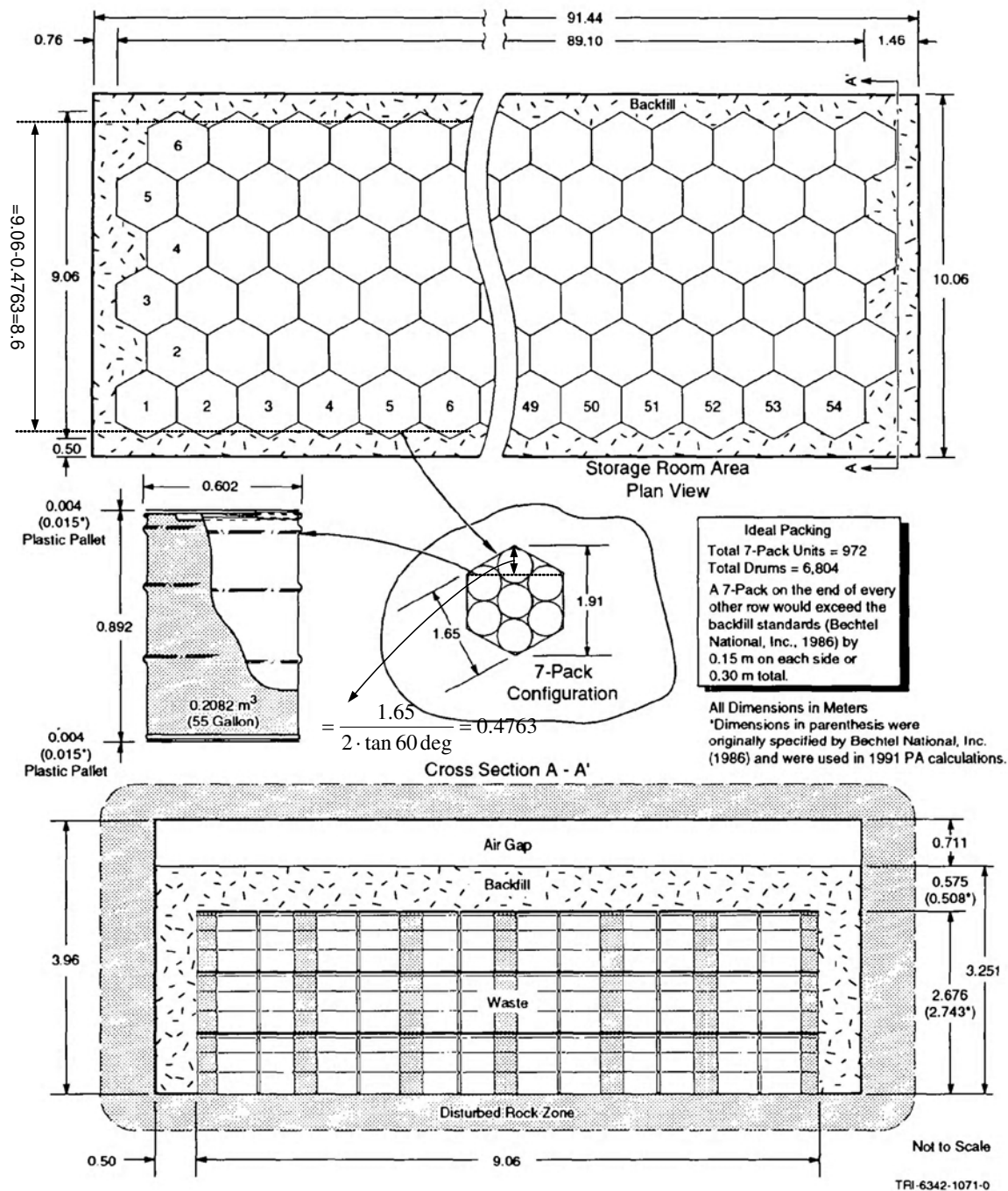
Figure 11: Ideal packing of drums in rooms and 10.06 m wide disposal room (Modified from Sandia, 1992, however, no backfill is modeled)

4   DRZ CRITERIA IN HALITE

The creation of the openings in salt that is initially under lithostatic stress, causes deviatoric stress states to develop and the salt begins to creep. Once disturbed, salt rocks will continue to creep as long as deviatoric stresses exist. Creep around unsupported openings will stop only after the opening is completely closed by creep and lithostatic stresses are reestablished in the salt. Despite the substantial deformations that accumulate by creep, there is little evidence to suggest the permeability is increased provided the deformation occurs through isovolumetric creep. However, deformation that results in an increase in the volume of salt (dilation) does result in increased permeability. In certain engineering situations, the actual quantification of permeability is secondary to determining the size and location of regions that experience the damage and increase permeability. The salt dilation zone, as a function of opening size and shape could be used as part of the design basis. Such an application could be used for evaluation of design options for seals at the WIPP (Van Sambeek, et al., 1993).

If the stress condition can be calculated using finite element or finite difference methods and appropriate material properties, the area around the opening that is expected to experience dilatancy can be defined through comparison of the calculated stresses with a stress-based dilatancy criterion during post-processing of the stresses. An example of the application of an engineering dilation criterion is shown in Figure 12 (Van Sambeek, et al., 1993). To develop this figure, the stresses around a rectangular opening situated in the WIPP stratigraphy were calculated using finite element modeling and WIPP material properties (Munson and DeVries, 1991). The calculated stresses were then processed to obtain a "damage" factor, D, considering the dilatancy criterion of Ratigan and Van Sambeek (1991).

Ratigan and Van Sambeek (1991) reported a linear dilatancy boundary as follows:

$$\sqrt{J_2} \geq 0.27I_1 = 0.81\sigma_m \tag{17}$$

where, I_1 = the first invariant of the stress tensor ($I_1 = 3\sigma_m$) and J_2 = the second invariant of the stress deviator as defined earlier by Equation 7.

Equation 17 was used to define a damage factor.

$$D = \frac{\sqrt{J_2}}{0.27I_1} \tag{18}$$

When $D > 1$, the shear stresses in the salt (J_2) are large compared to the mean stress (I_1) and dilatant behavior is expected. When $D < 1$, the shear stresses are small compared to the mean stress and dilatancy is not expected. The dark-shaded zone in Figure 12 shows the areas where dilant behavior is expected based on the calculated stresses. In Figure 12, a zone is also shown that highlights the area with damage factors between 0.8 and 1.0. While $D < 1$ suggests no dilatant behavior is expected, the stippled zone for

$0.8 < D < 1.0$ provides a somewhat more conservative indication of the potential of the disturbed zone.

In this analysis, Equation 17, the linear dilatancy boundary condition reported by Ratigan and Van Sambeek, is used for the DRZ criteria. To calculate the dilatant zone, the stress analyses results from SANTOS were post-processed using Equation 18. The post-processing ALGEBRA file to represent Equation 18 is provided in App. B. The healing effect of salt also was considered in this file.
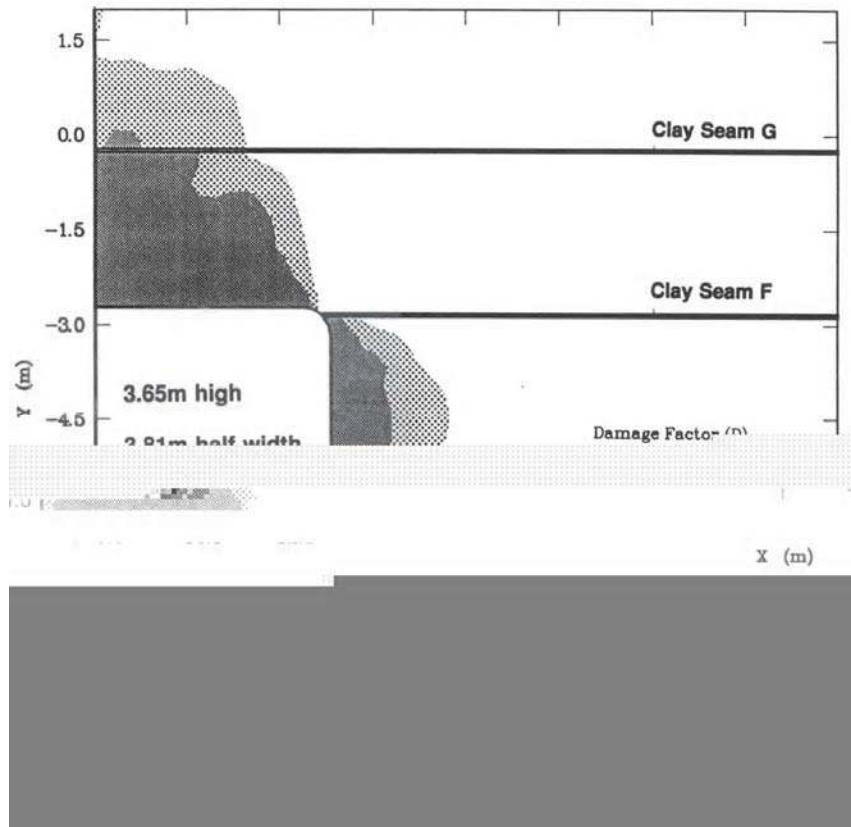
Figure 12: Calculated damage factors (D) around a 40-year-old rectangular opening within the WIPP stratigraphy consisting of salt, an anhydrite bed (MB 139), and three clay seams (Van Sambeek et al., 1993)

5   CALCULATION FLOW AND FILE NAMING CONVENTION

5.1 Computer Codes and Calculation Flow

FASTQ version 3.12 is used for generating the mesh to raise the disposal room by 2.43 m (Figure 10). The input file for the FASTQ mesh generation is provided in Appendix D. The FASTQ code is an interactive two-dimensional finite element mesh generation program. It is designed to provide a powerful and efficient tool to both reduce the time required of an analyst to generate a mesh, and to improve the capacity to generate good meshes in arbitrary geometries. It has a number of meshing techniques available. FASTQ has been designed to allow user flexibility and control. The user interface is built on a layered command level structure. Multiple utilities are provided for input, manipulation, and display of the geometric information, as well as for direct control, adjustment, and display of the generated mesh. Enhanced boundary flagging has been incorporated and multiple element types and output formats are supported. FASTQ includes adaptive meshing capabilities with error estimation, deformed and undeformed remeshing according to the error, element variable remapping, and some basic post-processing plotting (Blacker, 1988).

SANTOS version 2.1.7 is used for the solver in this analysis. The quasistatic, large-deformation finite element code SANTOS is capable of representing 2D planar or axi-symmetric solids (Stone, 1997b). The solution strategy, used to obtain the equilibrium states, is based on a self-adaptive, dynamic-relaxation solution scheme incorporating proportional damping. The explicit nature of the code means that no stiffness matrix is formed or factorized which results in a reduction in the amount of computer storage necessary for execution. The element used in SANTOS is a uniform-strain, 4-node, quadrilateral element with an hourglass control scheme to minimize the effects of spurious deformation modes. Finite strain constitutive models for many common engineering materials are available within the code. A robust master-slave contact algorithm for modeling arbitrary sliding contact is implemented. SANTOS, version 2.0.0, installed on the Sandia Cray J916 computer, was used for the earlier analysis. Recently, an executable SANTOS version 2.1.7 was installed on the Warthog workstation with the Linux operating system. The source code of SANTOS was copied to the workstation and compiled again. All of the verification and qualification test problems were exercised and documented in accordance with QA requirements. This SANTOS workstation version is used in this analysis.

BLOTII2 version 1.39 is used as the final post-processor. The disposal room creep closure, the DRZ boundaries, the shear failure zones and so on, are plotted using BLOT. BLOT is a graphics program for post-processing of finite element analyses output in the EXODUS database format. It is command driven with free-format input and can drive any graphics device supported by the Sandia Virtual Device Interface. BLOT produces mesh plots with various representations of the analysis output variables. The major mesh plot capabilities are deformed mesh plots, line contours, filled (painted) contours, vector plots of two/three variables (e.g., velocity vectors), and symbol plots of scalar variables (e.g., discrete cracks). Path lines of analysis variables can also be drawn on the mesh. BLOT's features include element selection by material, element birth and death, multiple

views for combining several displays on each plot, symmetry mirroring, and node and element numbering. BLOT can also produce X-Y curve plots of the analysis variables. BLOT generates time-versus-variable plots or variable-versus-variable plots. It also generates distance-versus-variable plots at selected time steps where the distance is the accumulated distance between pairs of nodes or element centers (Gilkey and Glick, 1991).

To calculate the volume change of the disposal room with time, NUMBERS version 1.19 is used. NUMBERS is a shell program that reads and stores data from a finite element model described in the EXODUS database format. Within this program are several utility routines that generate information about the finite element model. The utilities currently implemented in NUMBERS allow the analyst to determine information such as: (1) the volume and coordinate limits of each of the materials in the model; (2) the mass properties of the model; (3) the minimum, maximum, and average element volumes for each material; (4) the volume and change in volume of a cavity; (5) the nodes or elements that are within a specified distance from a user-defined point, line, or plane; (6) an estimate of the explicit central-difference time step for each material; (7) the validity of contact surfaces or slide lines, that is, whether two surfaces overlap at any point; and (8) the distance between two surfaces (Sjaardema, 1989).

These pre- and post-processing utilities are considered systems software and not subject to the requirements of NP 19-1 (memo 10/26/95 WPO# 27538 and WPO# 37416 for exceptions).

To calculate the porosity change in the room as a function of time, GNU AWK version 3.1.0 is used. The AWK converts the volume change of the disposal room into the porosity change with time. The AWK script is provided in App. C.

nSIGHTS version 2.01A is used for plotting the three-dimensional porosity surface. nSIGHTS (n-dimensional Statistical Inverse Graphical Hydraulic Test Simulator) is originally a comprehensive well test analysis software package. It provides a user-interface, a well test analysis model and many tools to analyze both field and simulated data. The well test analysis model simulates a single-phase, one-dimensional, radial/non-radial flow regime, with a borehole at the center of the modeled flow system. In this report, the function of plotting a 3D surface is the only feature used.

Figure 13 shows the computational flowchart for the Clay Seam G analyses.

FASTQ

Defines computational grid from stratigraphic model

SANTOS

Stress analyses for various f

ALGEBRA

- Converts time from seconds to years
- Converts stresses from Pa to MPa,
- Calculates DRZ boundary and shear failure zone in Anhydrite

NUMBERS

Calculates volume change of disposal room with time

BLOT

Plots disposal room creep closure, DRZ, shear failure zone, etc.

AWK

Converts volume change of disposal room into porosity change with time

nSIGHTS

Plots 3D porosity surface

Figure 13: Computational flowchart for Clay Seam G analyses

5.2 File Naming Convention

The general path for any of these subdirectories is: /**/clayg/. All of the files related to the analyses for the current room exist in the subdirectory of /**/clayg/current/ and ones related to the raised room are in the subdirectory of /**/clayg/raised/. All of the files that remain within each subdirectory are listed and described in Table 8.

The suffix the files, 0p0, 0p025, 0p05, 0p1, ..., etc. express the gas generation factors. For examples, the 0p0 means the gas generation factors is f=0.0, the 0p1 means f=0.1, the 1p2 means f=1.2 and so forth.

The name of FASTQ files is 0.00up.fsq and 2.43up.fsq. The 0.00up means unraised room, i.e. the current disposal room, and the 2.43up means a disposal room raised 2.43 m above the current level.

Table 8: File naming convention (* means wild card)

File Prefix/Suffix	File Definition
*.fsq	The FASTQ input files for the mesh generation
*.g	The FASTQ output files that will be used for the mesh file of SANTOS
clayg*.i	The SANTOS input files
clayg*.e	The SANTOS output files in the EXODUS database format
clayg*.o	The SANTOS output files in the ASCII format
initst_*.f	The user-supplied subroutine INITST to provide an initial stress state and the FPRES to provide the gas generation parameter, f, to SANTOS
initst_*.o	The object files from compiling the *.f
alg.alg	The ALGEBRA file to calculate the DRZ and the shear failure region
porosity.awk	The AWK file to calculate the porosity change in the room with time
*.num	The NUMBERS output file in the ASCII format to calculate the volume change of the disposal room with time from the SANTOS output files, *.e
normal*.txt	The normalized volume change of the disposal room from *.num
run*.log	The log file from SANTOS run
clayg*_pgas.dat	The result file of the gas pressure change in the disposal room
poro*.dat	The result file of the porosity change in the disposal room
PGAS_*_SNTS.xls	The excel file to adjust the gas pressure change data to the same number of time steps for plotting the gas pressure surface
Poro_*_SNTS.xls	The excel file to adjust the porosity change data to the same number of time steps for plotting the porosity surface
XYZ_*.dat	The three dimensional data for plotting the surfaces

6   ANALYSES PROCEDURE

The following procedures were performed to estimate whether raising the repository to Clay Seam G has any significant impact on the conceptual models used in performance assessment:

1. The effects of changing the code version on the calculated results were qualified by comparing the results for the current horizon using the SANTOS v.2.1.7 (also called the workstation (W/S) version) used in this analysis, with the one using SANTOS v.2.0.0 used by Stone (1997a). That means, first the baseline results provided by Stone (1997a) were replicated.

2. The effects of raising the room 2.43 m were calculated. The results of the disposal room being raised 2.43 m were compared with the baseline porosity surface results which are replicated for the current horizon by the SANTOS W/S version

3. Displacement data of the disposal room and wastes from SANTOS W/S version analyses were converted into the porosity data by ALGEBRA. A 3D porosity surface was made of these porosity data with the gas generation potential and time.

4. The structural implication of raising the room 2.43 m was evaluated by:

   o Comparing MB139 to a failure criterion

   o Examining stress conditions in the salt with respect to a damage function

7   ANALYSES RESULTS

The previous analyses using SANTOS, version 2.0.0 installed on the Sandia Cray J916, were carried out to a simulation time of 10,000 years by Stone (1997a). Analyses using SANTOS, version 2.1.7 installed on the Warthog with Linux OS, were carried out to the same simulation time. Thirteen cases of gas generation were investigated, these were for f=0.0, 0.025, 0.05, 0.1, 0.2, 0.4, 0.5, 0.6, 0.8, 1.0, 1.2, 1.6, and 2.0. The input file for one of the SANTOS analyses is included in Appendix E. The other input files are identical except for the title line. The gas generation parameter, f, is set in the user-supplied subroutine FPRES. The FPRES subroutine is used unchanged in this analysis. A sample FPRES subroutine for f=0.1 is given in Appendix F-1. Stone (1997a) used the user-supplied subroutine INITST to provide an initial stress state to SANTOS. In this analysis, the INITST subroutine is used unchanged from Stone (1997a). A sample INITST subroutine is also given in Appendix F-2. The gas pressure bleed-off by flow through the surrounding lithology is not permitted.

7.1 Comparison with Stone's Results

To identify the differences between the results of SANTOS version 2.1.7 and version 2.0.0, the analyses were carried out by SANTOS 2.1.7 using the input data, the FEM mesh, and related subroutine files that Stone (1997a) used. SANTOS was running on the Warthog Workstation.

The pressure changes in the disposal room with time for thirteen gas generation factors, f, are plotted as shown in Figure 14. The porosity histories are plotted as shown in Figure 15. Each line indicates the results obtained from version 2.0.0, and each symbol indicates the results obtained from version 2.1.7. The two results match well each other, which means the changes from version 2.0.0 to 2.1.7 of SANTOS had no effect on the results. This result further substantiates the results of the verification testing and provide assurance that use of SANTOS 2.1.7 is appropriate and consistent with calculations supporting the initial performance assessment for compliance application.
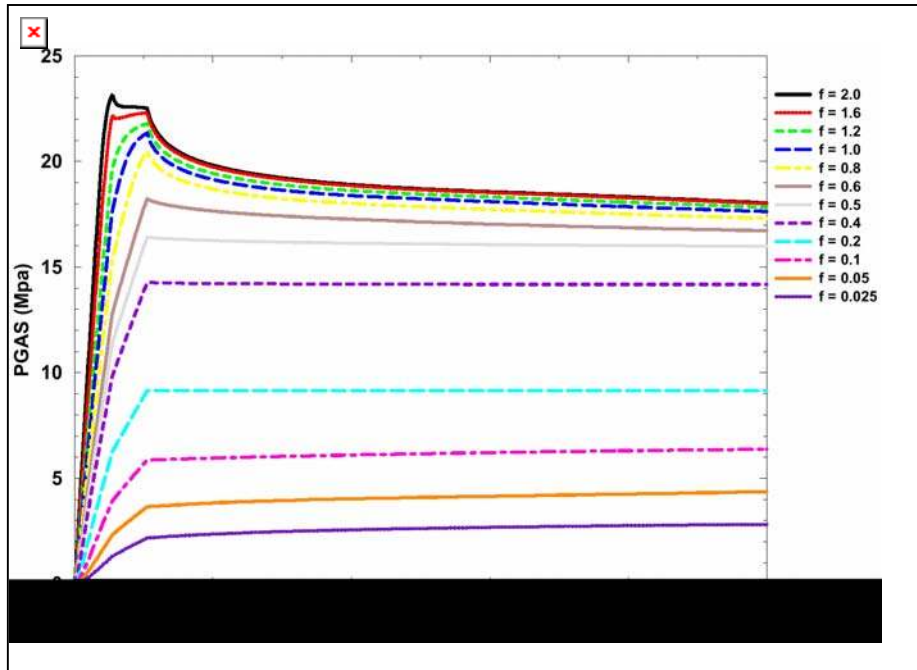
Figure 14: Pressure histories for various *f* by SANTOS version 2.0.0 and 2.1.7: Solid lines are for version 2.0.0 and symbols are for version 2.1.7
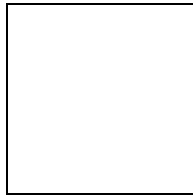
Figure 15: Porosity histories for various *f* by SANTOS version 2.0.0 and 2.1.7: Solid lines are for version 2.0.0 and symbols are for version 2.1.7

7.2 Creep Closure and Porosity Histories

7.2.1 Disposal room creep closure

The salt surrounding a disposal room will continue to creep as long as deviatoric stresses exist. Figures 16 to 19 show a close-up view of the deformed mesh around the disposal room being raised to the Clay Seam G with time, for $f = 0$, 0.4, 1, and 2 respectively.

Deformation in the absence of gas generation is shown Figure 16. The ceiling contacts the top of the waste due to the salt creep at approximately 25 years. The waste is compressed by the creeping salt after that. Most of the deformation has occurred during the first 1,000 years. After that, the deformation has slowed down considerably. The deformed shape clearly shows that the maximum compaction of the waste is due to vertical

41

closure of the room. At 300 years, the vertical closure has reached 91 percent of its maximum value. The horizontal contact of the rib with the waste occurs at approximately 150 years. At 10,000 years, the waste has been compacted somewhat by the horizontal closure of the rib but not significantly compared to the vertical compaction.

The closure of the disposal room at 0, 10, 25, 300, 1000, 10000 years for $f = 0.4$ is shown in Figure 17. As seen in the figures, the compaction of the waste is entirely due to the vertical room closure, since the deforming rib does not contact the waste at any time during the simulation. The gas generation is such that the room porosity is the same at 300 years as it is at 10,000 years. The gas pressure essentially balances the overburden load so that the vertical closure of the disposal room becomes constant.

In the case of $f=1.0$ as shown in Figure 18, the roof of the room contacted the top of the waste at approximately 30 years, which is later than the case of $f=0.4$. The creep is much slower than the case of $f=0.4$ due to the generated gas pressure. The roof is beginning to separate from the waste at 1,000 years and thereafter inflates. Note: Response of this model does not capture the physical reality of hydrofracture propagation of high pressure away from the repository.

In the case of $f=2.0$ as shown in Figure 19, the creep is much slower than the case of $f=1.0$. The inflation of the room at 1,000 years is much larger than in the case of $f=1.0$, again hydrofracture is not represented in these analyses. The volume of the disposal room at 10,000 years becomes almost the same as the volume at 0 years.

The four figures show that the large deformations result in the contact of the roof and floor with the ribs at the corners of the room. The contact in the corners of the disposal room is an important feature of the analyses and can be captured using the arbitrary contact surface capability of SANTOS. The roof and floor are either in contact with the waste or in contact with the ribs, which means that no significant void spaces are developed. This deformation mode results in a minimum free volume in the room.

In conclusion, the volume change of the disposal room is strongly dependent on the gas generation factor, f.
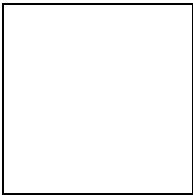
Figure 16: Close-up view of the deformed disposal room containing the waste with time for f=0.0

0 year   **10 years**   **25 years**

Argillaceous Halite
Clean Halite
Anhydrite
Waste

10,000 years   **1,000 years**   **300 years**
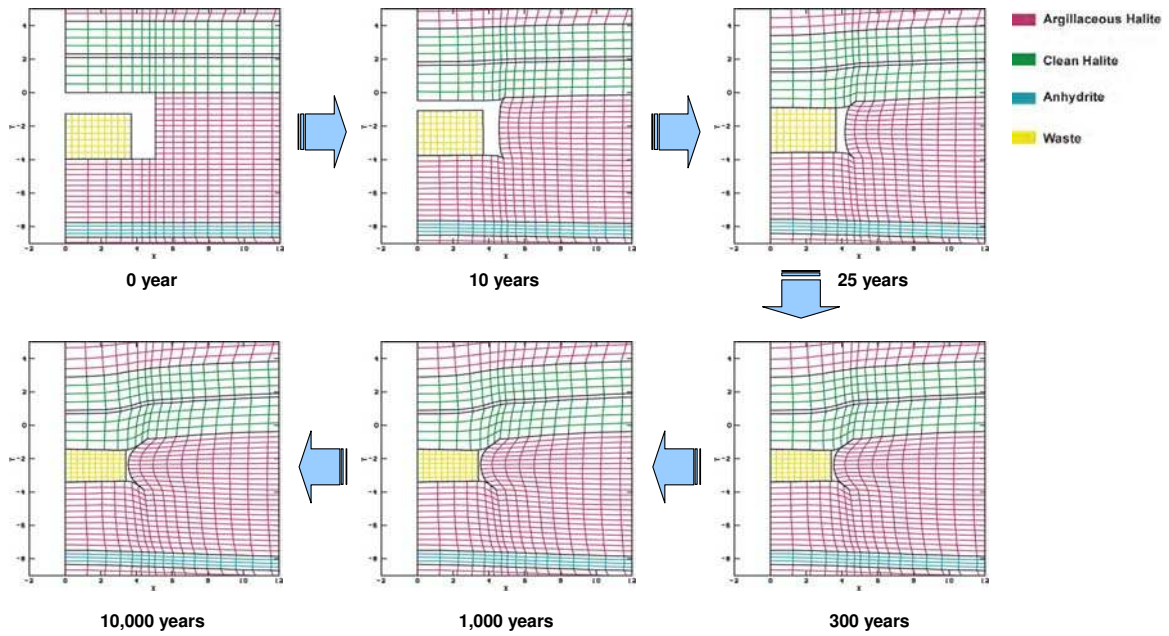
Figure 17: Close-up view of the deformed disposal room containing the waste with time for *f*=0.4
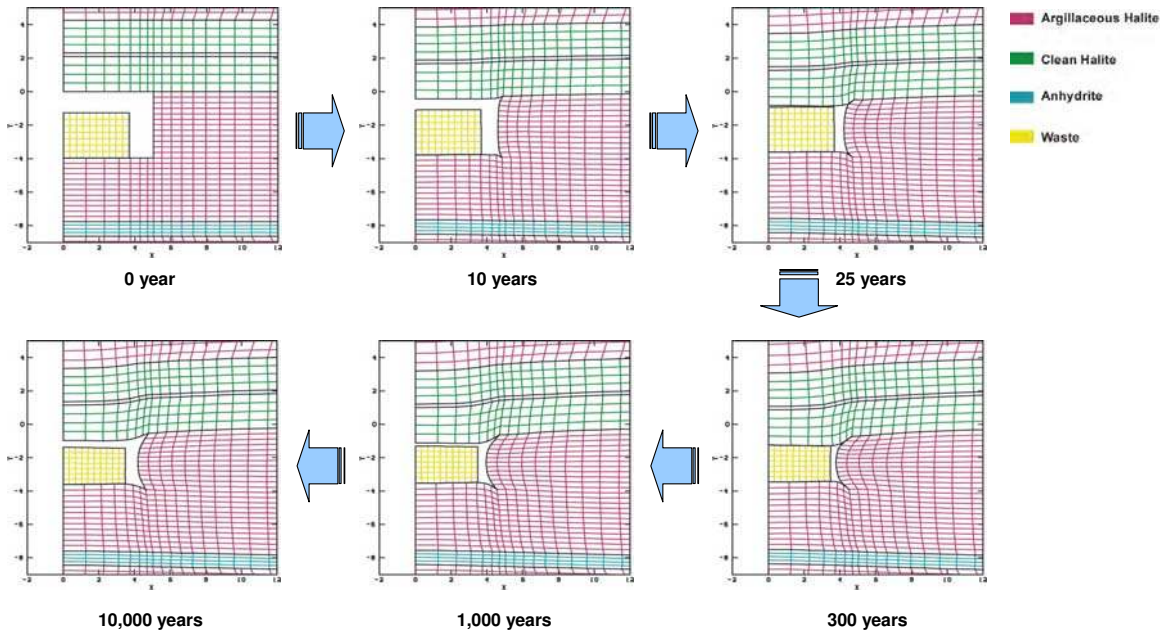
Figure 18: Close-up view of the deformed disposal room containing the waste with time for *f*=1.0
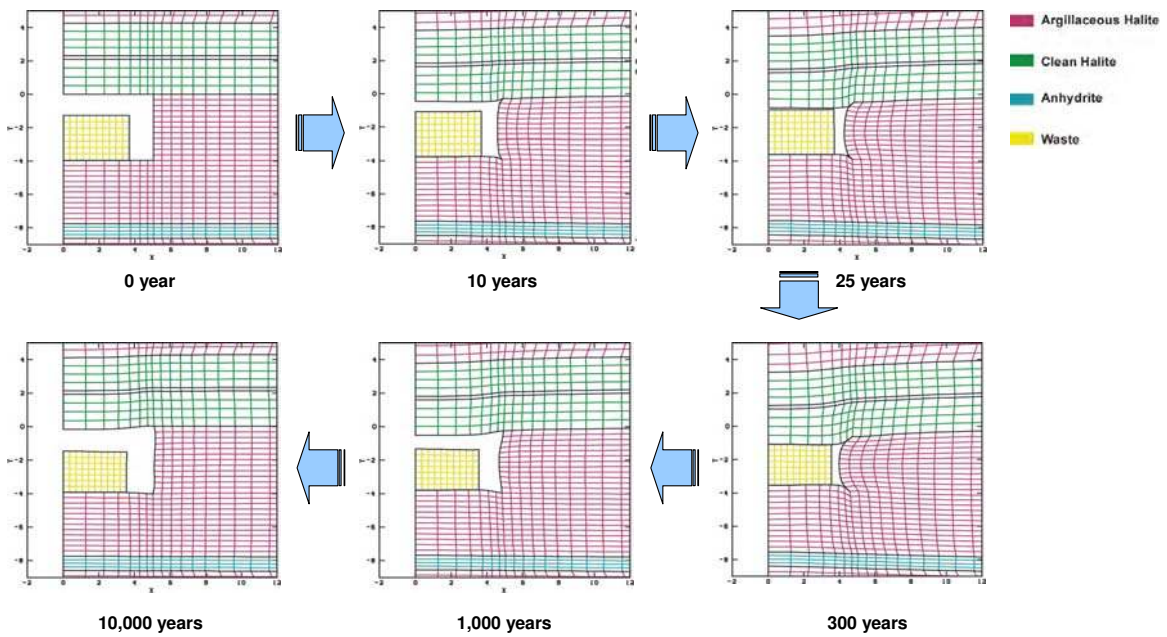
Figure 19: Close-up view of the deformed disposal room containing the waste with time for *f*=2.0

7.2.2 Pressure and Porosity histories

One of the most interesting results from the analyses is the pressure buildup in the disposal room and the corresponding room porosity. Figure 20 shows the disposal room pressure histories for the various values of gas generation parameter, f. Obviously for f=0, the amount of gas generation is zero resulting in a nominally zero pressure in the room for all time. As would be expected in all other cases, the room pressure rises during the gas generation period of 1,050 years. Thereafter in time, there appears to be a transition in the character of the response at about f=0.4. For f values greater than 0.4, the room pressure begins to drop from its maximum value after gas generation stops, and for values less than 0.4, the room pressure remains constant at its maximum value throughout the 10,000 year simulation. For example with f=1.0 (full gas generation) the room pressure increases monotonically during the period of gas generation and reaches a value slightly larger than 21 MPa at 1,050 years. When the gas generation ceases at this time, the room pressure begins to drop, reaching a value of approximately 17.5 MPa at 10,000 years. For the highest values of f (1.6 and 2.0), there is very little difference in the maximum pressure reached, approximately 23 MPa at 550 years. The pressure drops dramatically to 18 MPa at 10,000 years and still appears to be decreasing as the internal gas pressure and overburden approach equilibrium. On the other end of the range for f, an interesting case is f=0.025 (i.e., 2.5 percent of full gas generation). The figure clearly shows that for even this small amount of gas generation, the pressure in the room rises significantly (2.9 MPa at the end of 10,000 years) to approximately 20 % of the value of the lithostatic stress at the repository horizon.

Figure 21 shows the disposal room porosity histories for the thirteen cases of gas generation considered. As would be expected, the room porosity drops monotonically from its initial value of approximately 85 percent during the first 100 to 500 years, depending on the value of f. Thereafter, once again, there appears to be a transition in response at about f=0.4. For values of f below that value, the porosity continues to decrease with time but at a slower rate, as equilibrium is reached between the internal gas pressure and the salt overburden. For values of f greater than 0.4, the porosity starts to increase after reaching a minimum value. In fact, for the gas generation case of f=2.0, the room actually inflates to a porosity of about 85 percent at the end of the simulation, which is nearly equal to the original porosity. The porosity reached at this same time for the case without any gas generation, f=0, is approximately 22.7 percent.
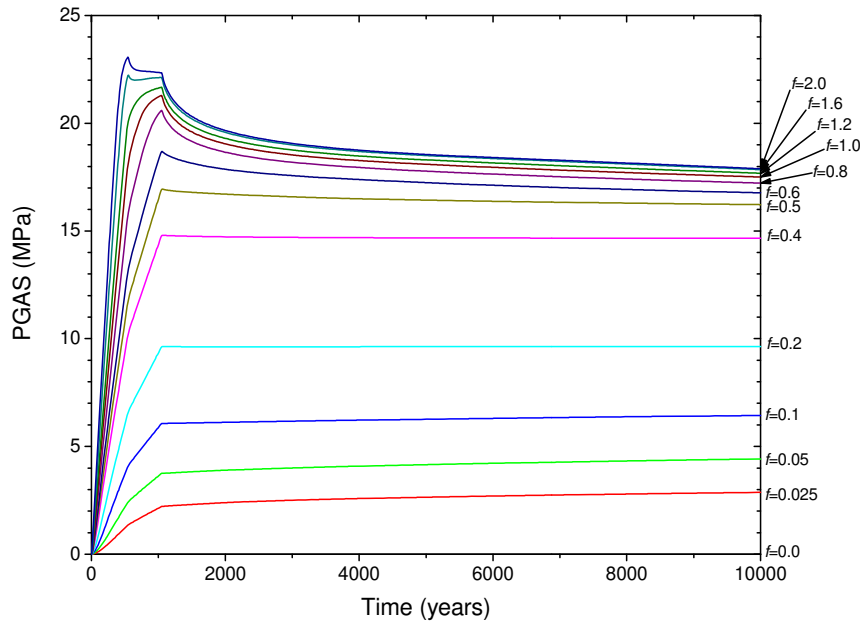
Figure 20: Pressure histories for various values of the gas generation factor, *f*, for a disposal room being raised to the Clay Seam G, containing the waste without backfill.
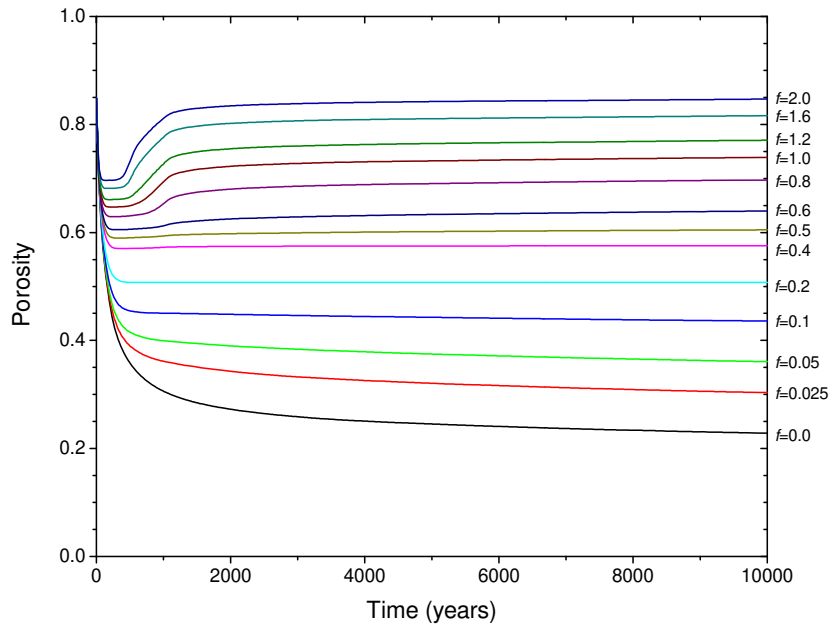
Figure 21: Porosity histories for various values of the gas generation factor, *f*, for a disposal room being raised to the Clay Seam G, containing the waste without backfill

7.2.3 The effect of raising the room 2.43 m

In this section, the results for the disposal room raised 2.43 m above the present level are compared with the results for the room at the present level to examine possible structural effects.

The pressure histories in a room for various values of the gas generation factor, f, are compared with each other as shown in Figures 22 and 23. Each line indicates the pressure change in the disposal room at the present level, and each symbol indicates the pressure change in the disposal room raised 2.43 m above the present level. The two results coincide well with each other for f=0 to 0.1. The pressures of the raised room are slightly higher than the present room for f=0.2 to 0.5. For f=0.6 to 2.0, the pressures of the raised room are slightly higher initially; however, the pressures of the raised room become lower than the present room after a certain time. In the case of f=0.6, the transition point is about 8,000 years. In the case of f=2.0, the transition point is 550 years at which the highest pressure is reached. However, the differences are very small from an overall point of view.

The porosity histories in a room for various values of the gas generation factor, f, are compared with each other as shown in Figures 24 and 25. Each line indicates the results for the present room, and each symbol indicates the results for the raised room. For f=0 to 0.5, the porosities of the raised room are lower than the current room's for the entire analysis period. For f=0.6 to 2.0, the porosities of the raised room are lower for the short term however, the two sets of porosities become the same after a certain time. The transition point is about 8,000 years for f=0.6. In the case of f=2.0, the transition point is 550 years. However, all of the differences are less than 5%. This means the effect of raising the room 2.43 m is very small on the porosity changes in the room.

In the case of f=0.0 and 0.025, the pressure histories of the current room are almost same as the ones of the raised room, while the porosity histories of the raised room are lower than the current room's. In the case of f=0.2, 0.4, and 0.5, the pressure histories of the raised room are higher than the current room's while the porosity histories of the raised room are lower than the current room's. It seems to be the higher pressure should coincide with higher porosity. However, the initial porosity is changed by the deformation of the disposal room due to salt creep closure. The material all around the current room is the argillaceous salt while the material of the roof of the raised room is the clean salt as shown Figure 6. The creep properties of the clean salt and the argillaceous salt are different as shown Table 3. In addition, the floor is separated from the underlying Marker Bed 139 by 3.81 m instead of 1.38 m and the additional salt is increases closure slightly. Thus, the deformation tendencies of the disposal rooms are slightly different and account for this minor variation. The porosity history is affected by the deformation characteristics of the material around the room as well as the gas pressure.
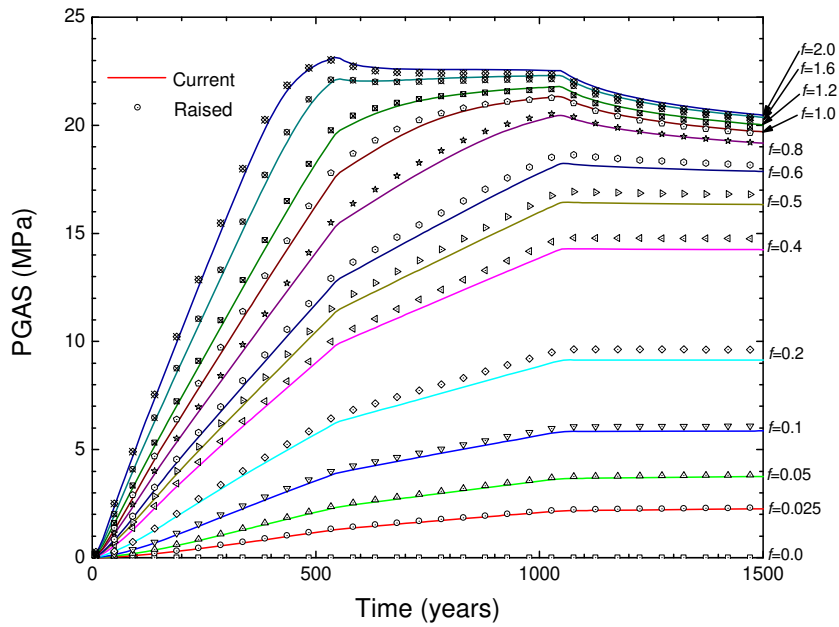
Figure 22: Pressure histories for disposal rooms to 1500 years: Solid lines are for current room and symbols are for raised room
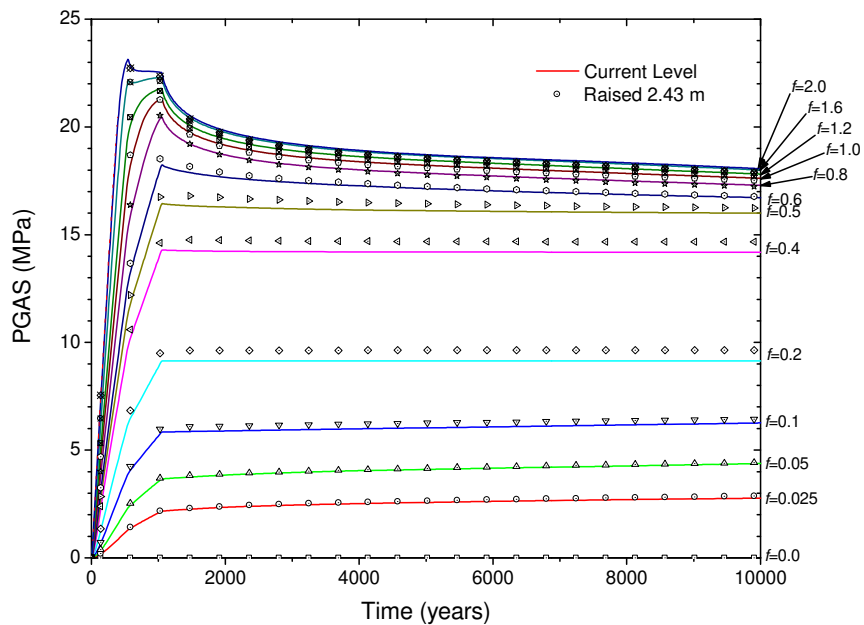
Figure 23: Pressure histories for disposal rooms to 10,000 years: Solid lines are for current room and symbols are for raised room

48
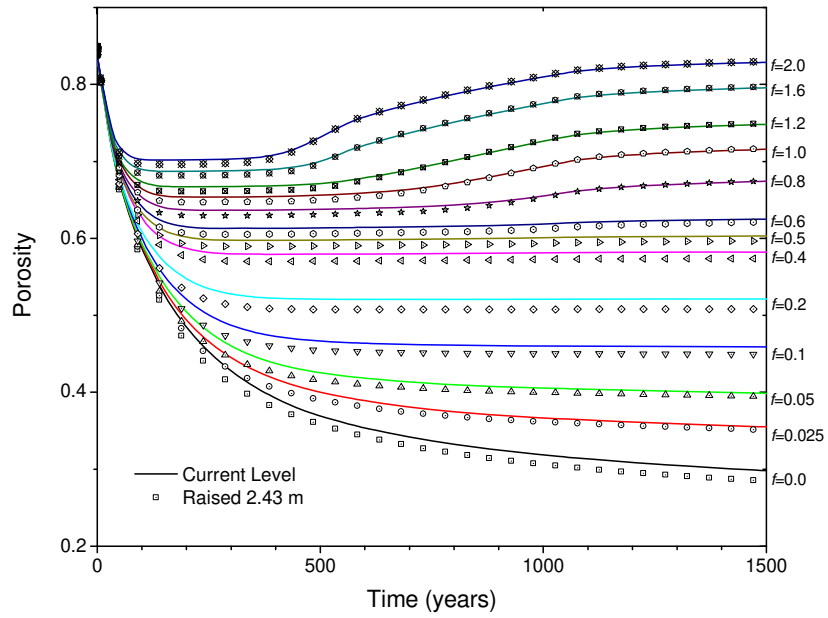
Figure 24: Porosity histories for disposal rooms to 1,500 years: Solid lines are for current room and symbols are for raised room
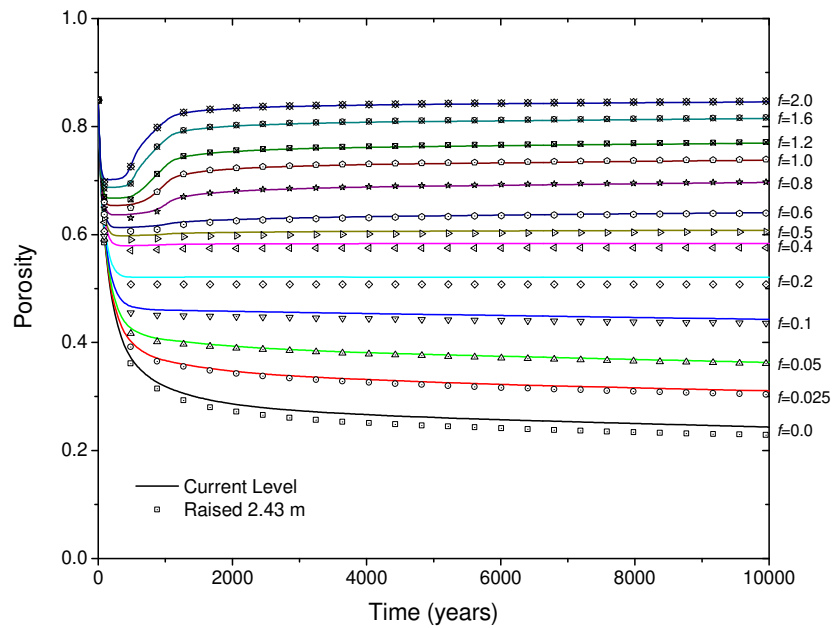
Figure 25: Porosity histories for disposal rooms to 10,000 years: Solid lines are for current room and symbols are for raised room

7.3 Porosity Surface

The pressure and porosity histories in Figure 22 and 24 are converted into the surface in the three-dimensional space as shown in Figure 26, so called a porosity surface like that shown in Figure 1. Figure 26 shows the changes of the porosity and pressure in the disposal room being raised 2.43 m with the gas generation factors and time. The porosity surface data will be provided for BRAGFLO analyses (refer to Figure 2).

The change of porosities with the gas generation factors and time is plotted again on a log time scale as shown in Figure 27. Figure 28 displays the porosity difference between the two porosity changes with the gas generation factors and time in the raised room and the current room. Considering the range of f from 0.07 to 0.99 (refer to App. A-5) as used in the BRAGFLO calculations to study the effects of gas on the flow of brine through the repository and up an intrusion borehole, the differences between the two surfaces are less than 5%. This means the effect of raising the room by 2.43 m on the porosity surface is inconsequential.
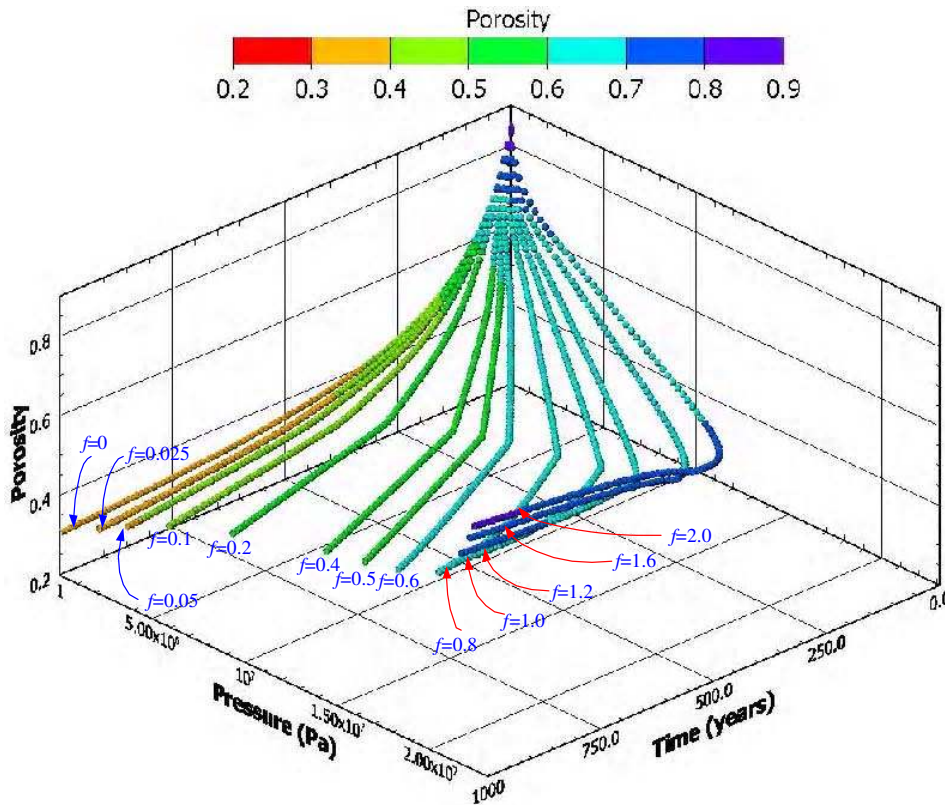
Figure 26: Porosity surface for disposal room raised 2.43 m above the current level
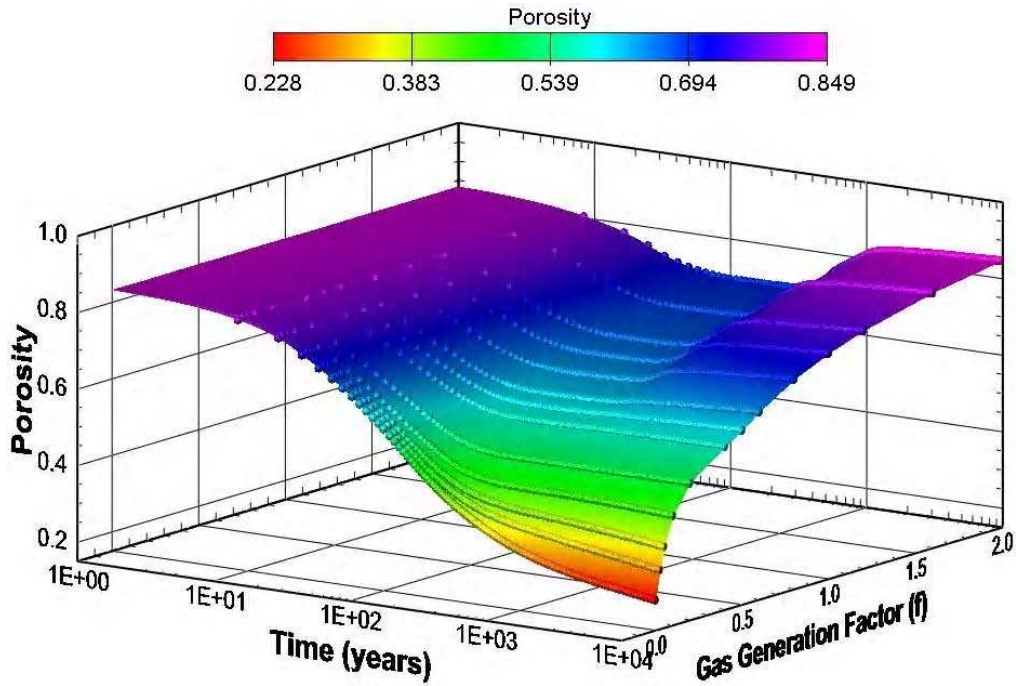
Figure 27: The change of porosities with the gas generation factors and time for disposal room raised 2.43 m above the current level (log time scale)
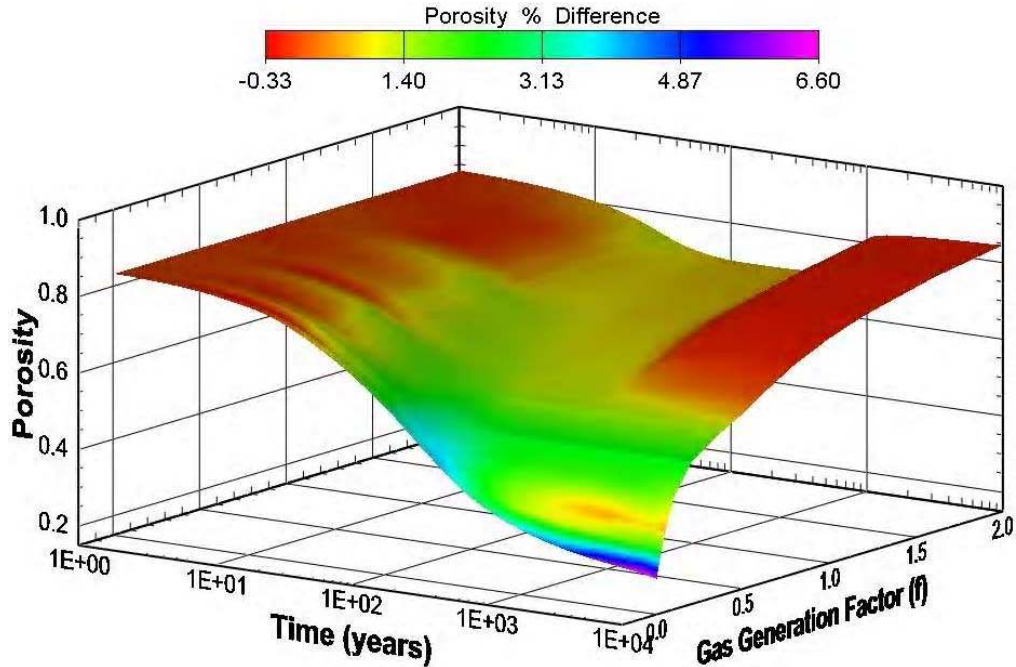
Figure 28: The change of porosity difference between the raised room and the current room (log time scale, %)

7.4 DRZ

Excavation of the repository and the consequent release of lithostatic stress create a disturbed rock zone (DRZ) around the underground openings. Fractures and microfractures within the DRZ increase porosity and permeability of the rock and could provide avenues for brine flow from the DRZ to the excavated opening. Salt creep is expected to close the fractures in the halite in the DRZ over time, exhibiting what is called the healing effect. In this section, the change of DRZ with time is provided through the interpretation of the SANTOS analyses results.

Figures 29 through 32 show the change with time of the DRZ around a disposal room raised 2.43 m above the current level for the gas generation factor f=0.0, 0.4, 1.0 and 2.0. The undisturbed zone (dark blue zone) in the figures is defined by $D < 1$ in Equation 18 in Section 4. The most extensive DRZ occurs at early time, say in the first ten years after the opening is mined. As the back stress — caused by resistance to deformation of the waste stack — increases, the DRZ disappears according to the stress invariant criterion. The undisturbed zone no longer appears after the last time frame (6th frame) in the figures. This finding is consistent with other similar numerical simulations, such as Van Sambeek et al. (1993). They reported "A similar calculation for a brine-filled borehole or internally pressurized cavern shows that the thickness of the dilatancy zone depends on the internal pressure. The dilatancy zone around a cavern can be completely suppressed by an internal pressure equal to a small fraction of the lithostatic stress for the depth of the cavern." Thus, calculations show that the damaged zone within the salt would heal.

The maximum extent of the DRZ calculated for the raised repository reaches approximately 3.8 m, the distance to the anhydrite layer (MB 139), below the room. The DRZ does not extend through the anhydrite layer that behaves as a buffer. The DRZ above the room disappears within a short period after the ceiling of room contacts the waste.

Modeling of the raised repository can be compared to Figures 33 to 36, which show the change of the DRZ around a disposal room at the current horizon with time for f=0.0, 0.4, 1.0 and 2.0. The largest DRZ occurs early after the excavation for all f values, which is very similar to the case for the raised repository. The DRZ under the room does not extend through the anhydrite layer, in a manner similar to what happens in the case of the raised room. A maximum thickness of the DRZ is approximately 3.6 m over the roof of the room. The thickness of the DRZ in the floor of the present room is 1.4 m, the distance to the anhydrite layer. The DRZ does not extend through MB 139, the same as the case of the raised rooms.

In these calculations, gas production from corrosion and microbial activity initiates instantaneously. Internal gas pressure is a key concern when considering the DRZ evolution and devolution in terms of the modeling output. As noted previously, rooms in which no gas or minimal gas is produced will close completely around the waste, as shown in Figures 29 and 33. Gas production from inside the room affects room closure and characteristics of the DRZ. The stress conditions thus created in the rock salt would appear favorable for healing to occur, but it may be that healing would not occur because gas has entered the void space. If the inward creeping rock salt does not experience a solid, me-

chanical back stress, it will not heal. These concepts need to be taken into account when examining the DRZ figures, in which the DRZ is delineated based on the invariant stress criterion.

The vertical closure would evidently be sufficient to create a back stress in the vertical direction for all gas generation factors considered. The upper and lower salt DRZ would thereby be situated in a stress field favorable for healing. The rib deformation, based on these models, is not sufficient to compress the waste laterally when gas is produced within the room.

Undisturbed Zone:

$$\sqrt{J_2} \le 0.27 \cdot I_1$$
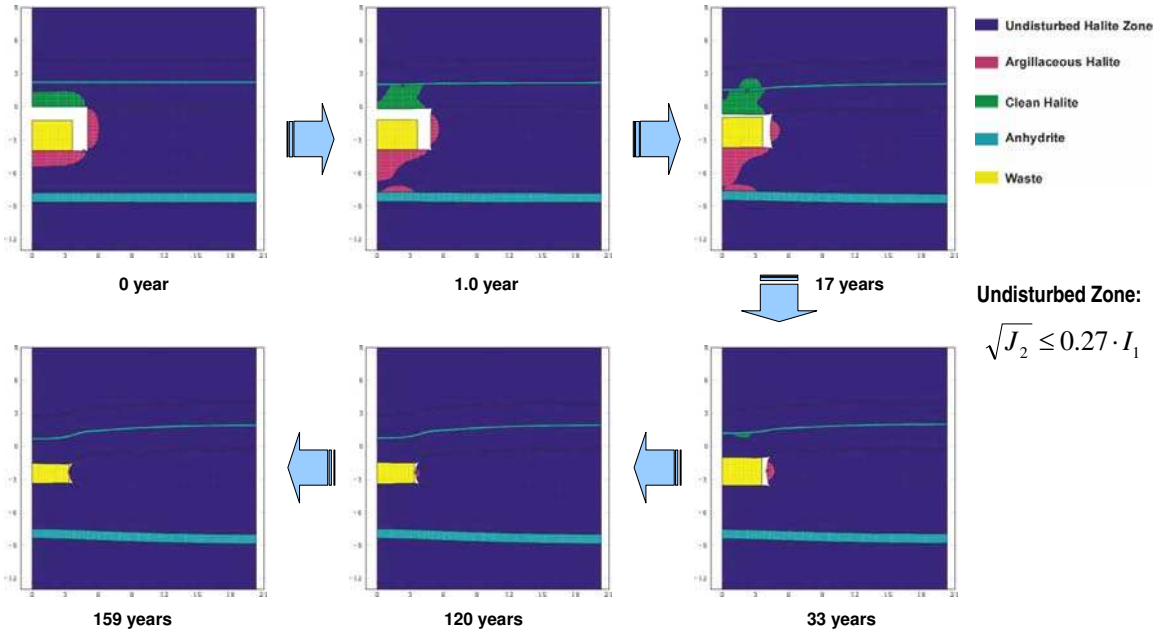
Figure 29: Change of the DRZ around a disposal room raised 2.43 m above the current level for the gas generation factor f=0.0.

Undisturbed Zone:

$$\sqrt{J_2} \le 0.27 \cdot I_1$$
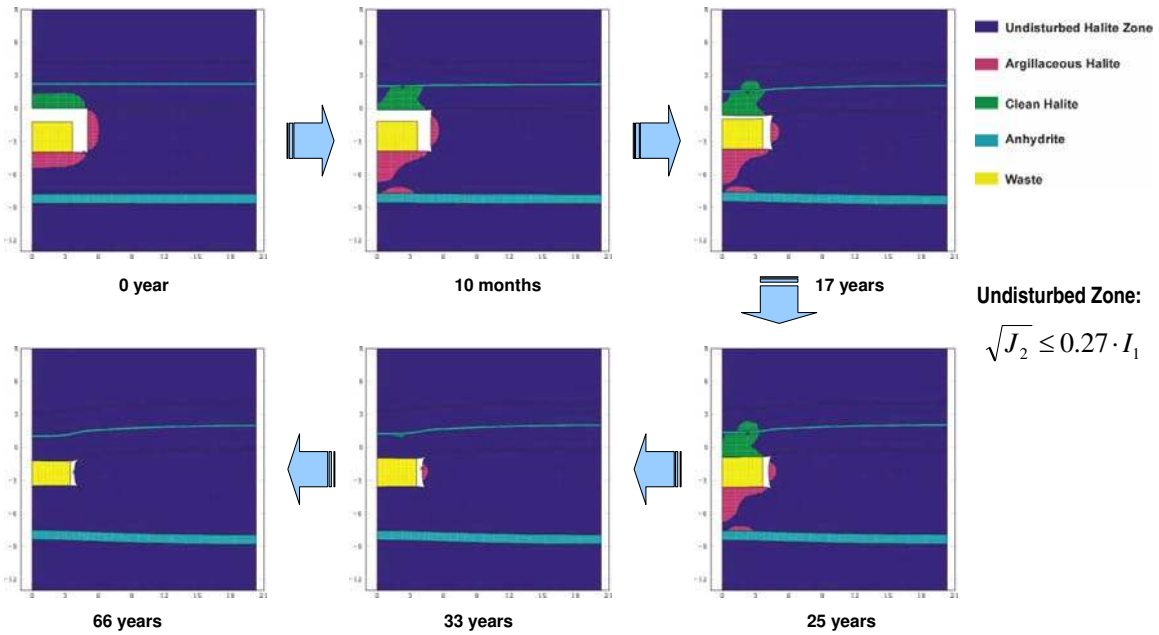
Figure 30: Change of the DRZ around a disposal room raised 2.43 m above the current level for the gas generation factor f=0.4.
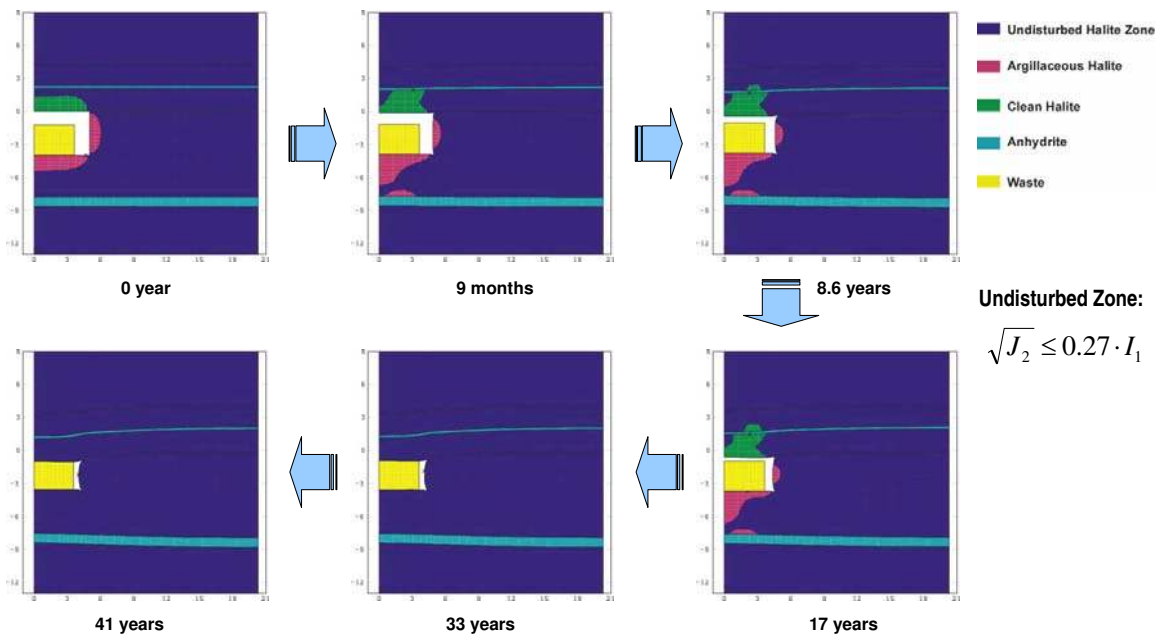
Figure 31: Change of the DRZ around a disposal room raised 2.43 m above the current level for the gas generation factor f=1.0.
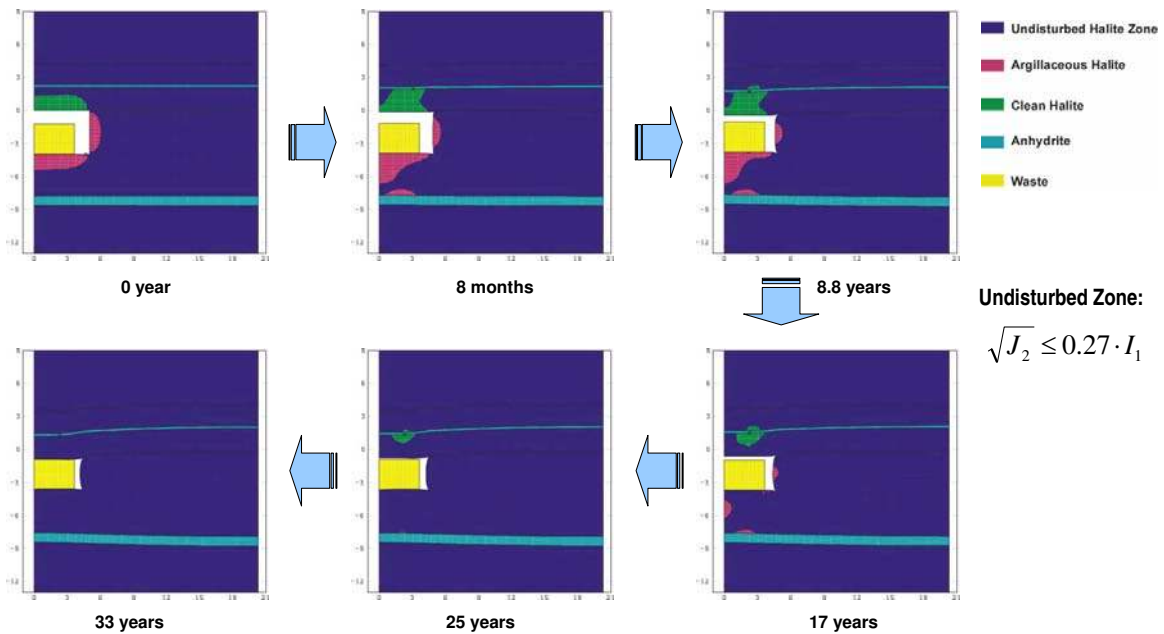
Figure 32: Change of the DRZ around a disposal room raised 2.43 m above the current level for the gas generation factor f=2.0.
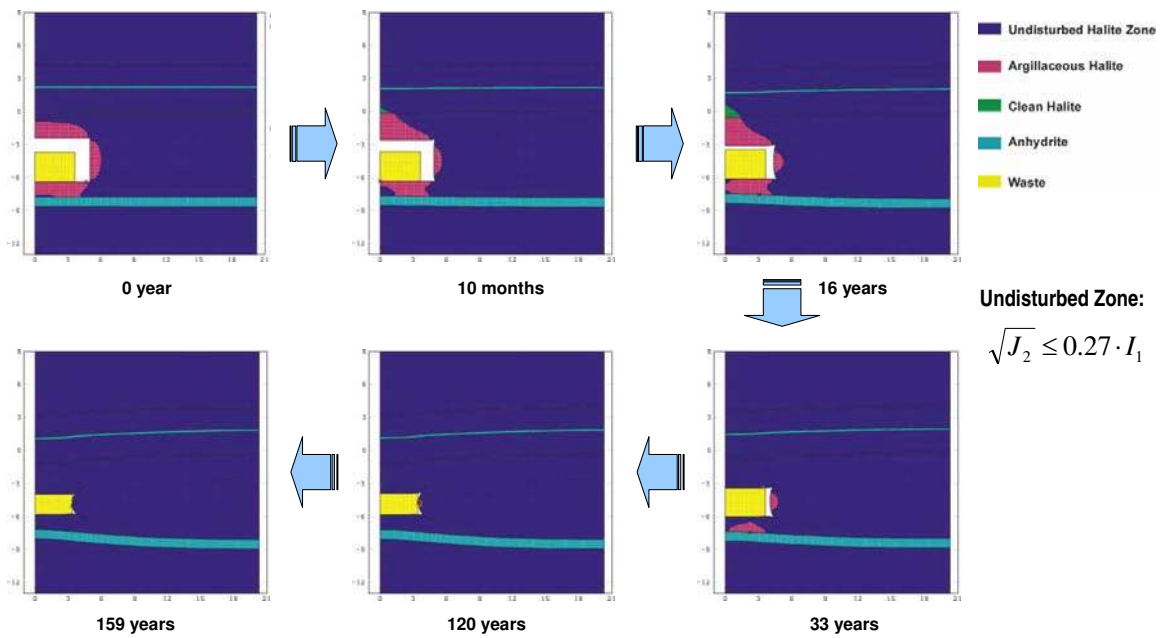
Figure 33: Change of the DRZ around a current disposal room for the gas generation factor f=0.0.
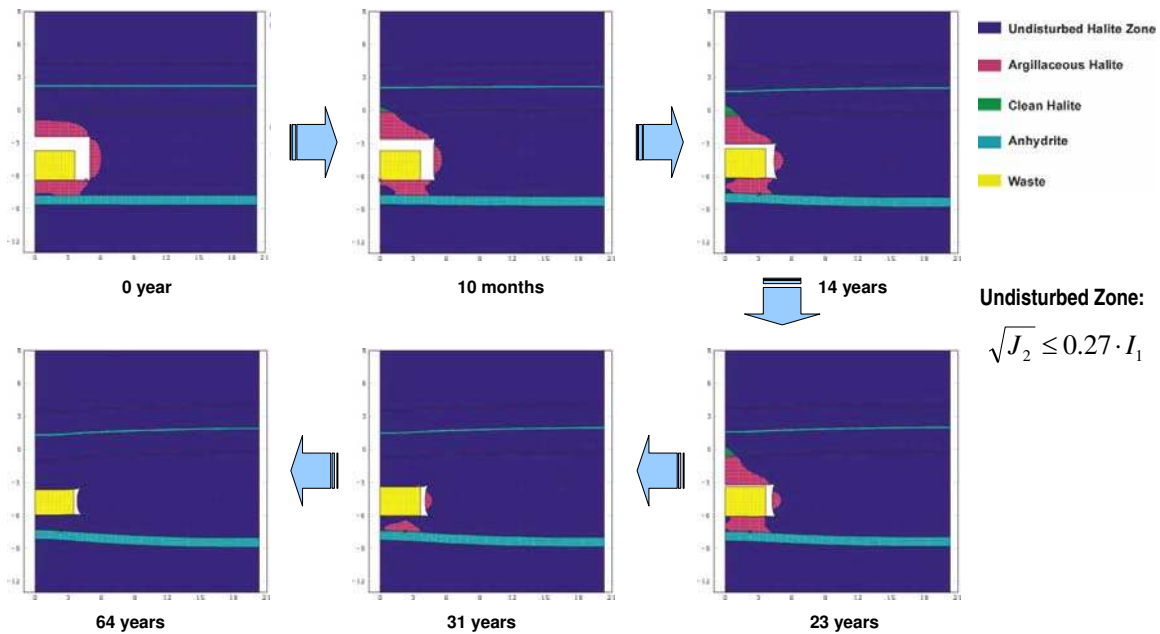
Figure 34: Change of the DRZ around a current disposal room for the gas generation factor f=0.4.
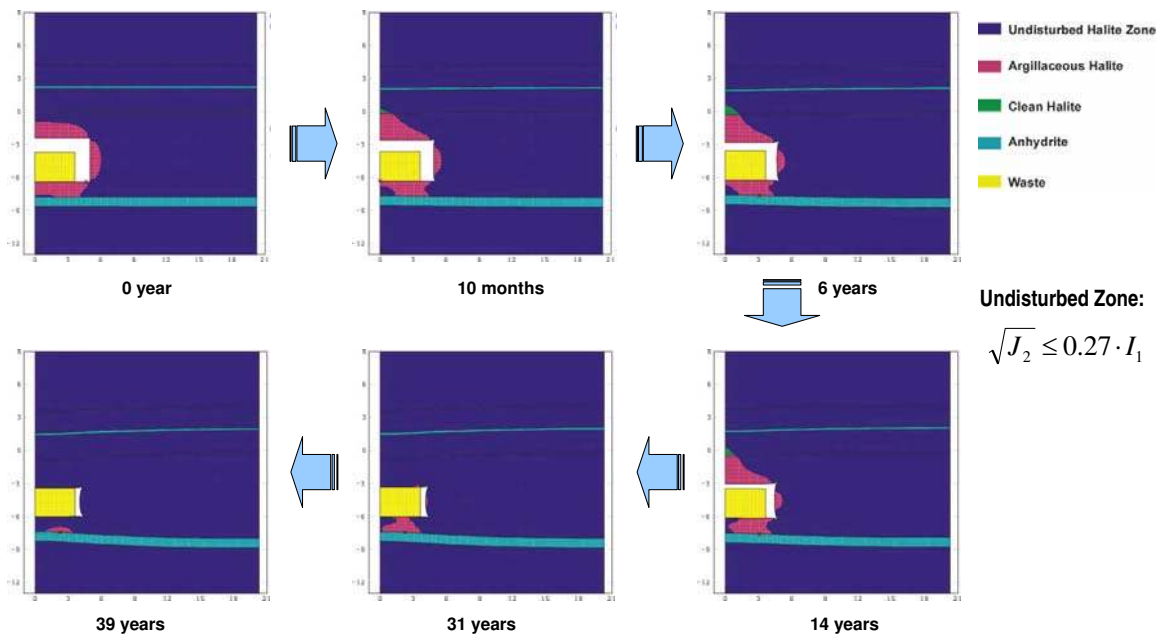
Figure 35: Change of the DRZ around a current disposal room for the gas generation factor f=1.0.
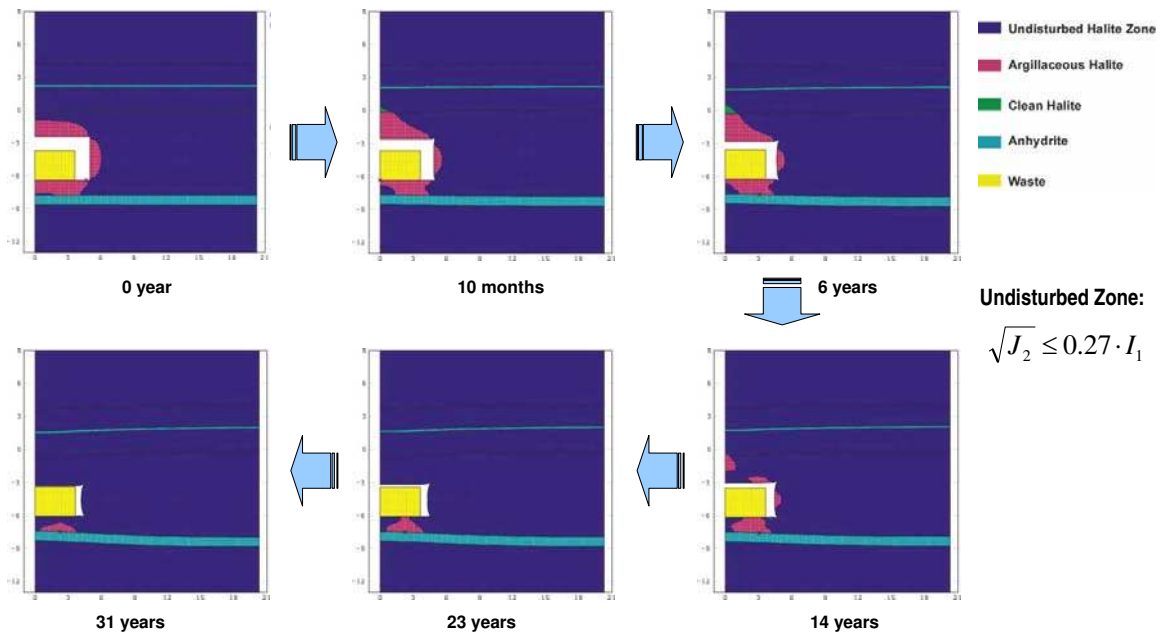
Figure 36: Change of the DRZ around a current disposal room for the gas generation factor f=2.0.

7.5 Shear Failures in Anhydrite

In this section, as discussed in Section 2.2.4, the shear failure pattern with time in the anhydrite is interpreted from the SANTOS output using the Drucker-Prager criterion. In the case of anhydrite, it is assumed that if MSF<1, the shear failure will have occurred, and the tensile strength is zero. The MSF is the cumulative shear failure variable which is defined from Equation (12):

$$SF = \frac{C - aJ_1}{\sqrt{J_2}} \tag{19}$$

$$MSF = Min\ (SF) \tag{20}$$

MSF is the minimum value of SF over all previous time steps. It is defined in this manner because, unlike salt, once the anhydrite fails, it does not heal.

Figures 37 to 40 show the shear failure zones with time in the upper and the lower anhydrite layers of the disposal room being raised 2.43 m. The shear failure does not occur in either the upper or lower anhydrite layers at the moment of excavation, but appears above and below the middle of the pillar one day after excavation. The shear stress in the anhydrite increases with time, therefore the extent of the failure zone also increases. The maximum extent of the shear failure zone occurs within the first 100 years. The internal gas pressure of the room does not affect the size of the failure zone in the anhydrite.

Figures 41 to 44 show the shear failure zone with time in the upper and the lower anhydrite layers of the present disposal room. The failure pattern of the present room is similar to the one of the raised room except the shear stress in the anhydrite for the present room increases faster than the raised room.

The distance between the bottom of the disposal room and the lower anhydrite layer is increased from 1.38 m to 3.81 m due to raising the room by 2.43 m. In other words, the current room is closer to Marker Bed 139. Because of this, the deformation of the anhydrite layer with the room closure is larger for the current room than the raised room. The shear failure zone is accordingly larger for the current room as shown in Figure 37 to 44.
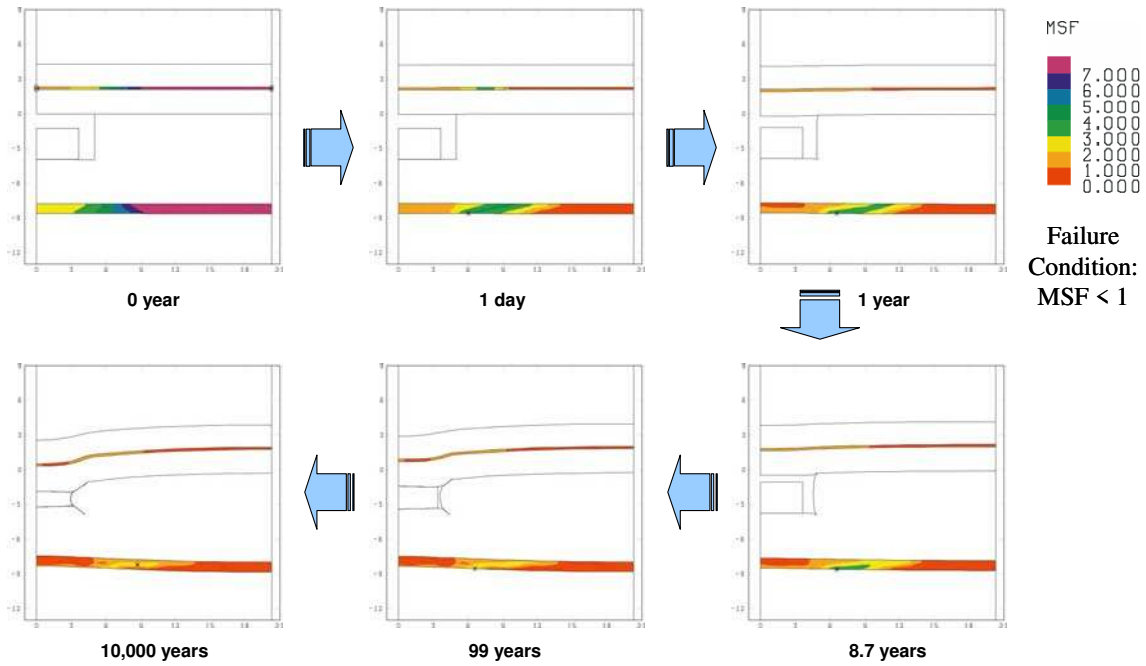
Figure 37: Changes of the shear failure zone with time in the upper and the lower anhydrite layers of the disposal room being raised 2.43 m, f=0.0.
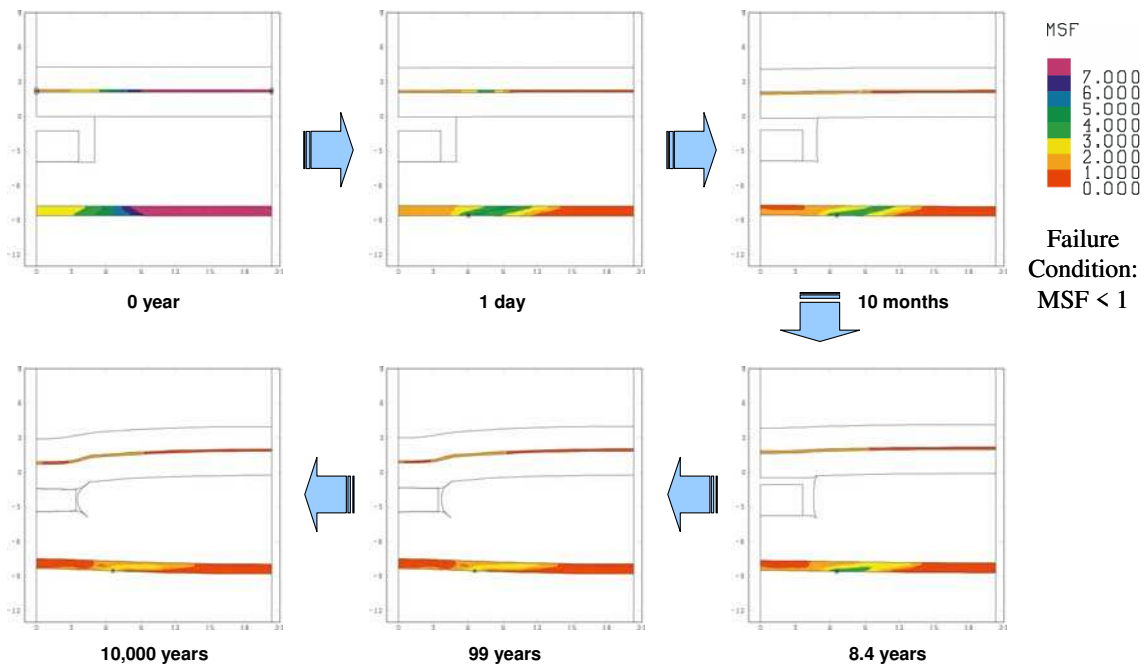
Figure 38: Changes of the shear failure zone with time in the upper and the lower anhydrite layers of the disposal room being raised 2.43 m, f=0.4.
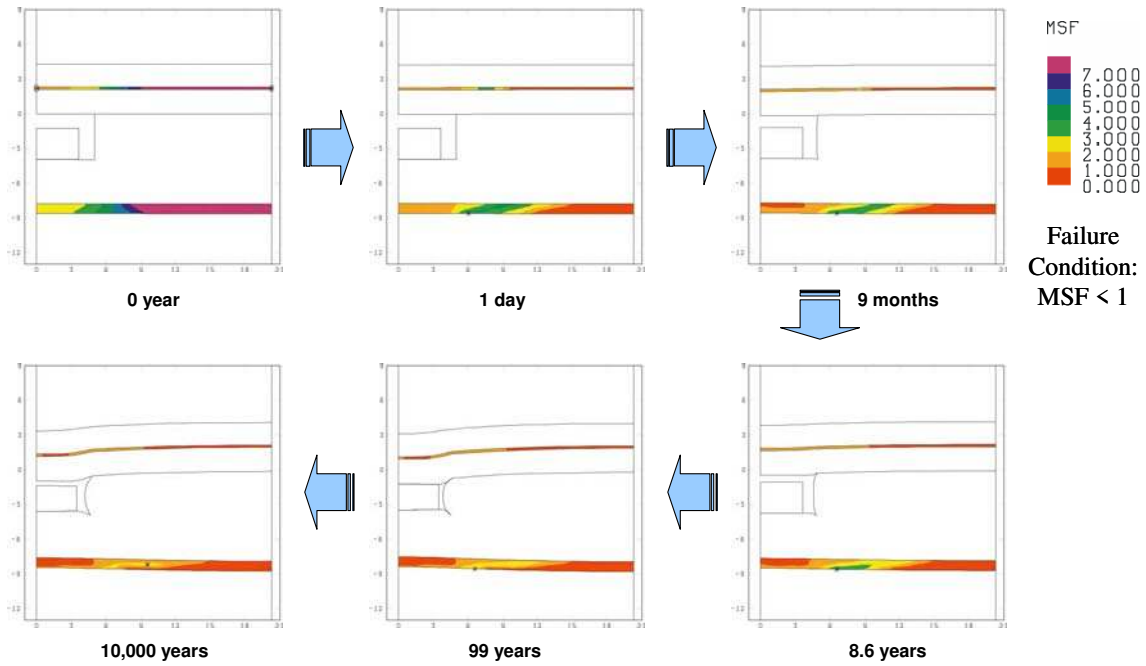
Figure 39: Changes of the shear failure zone with time in the upper and the lower anhydrite layers of the disposal room being raised 2.43 m, f=1.0.
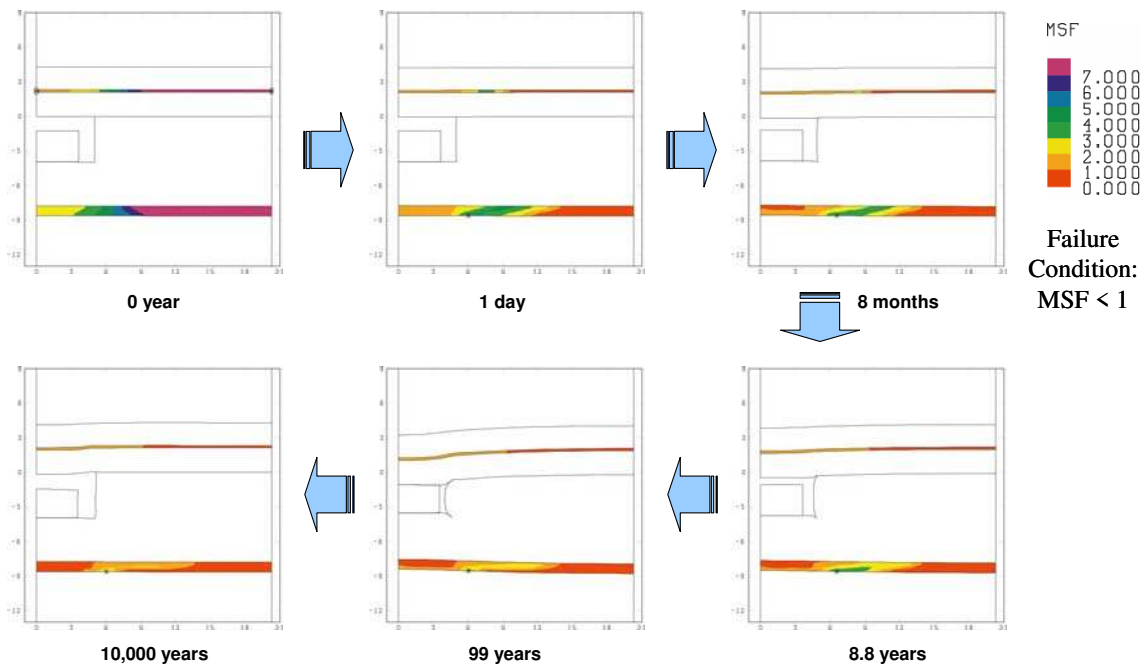
Figure 40: Changes of the shear failure zone with time in the upper and the lower anhydrite layers of the disposal room being raised 2.43 m, f=2.0.
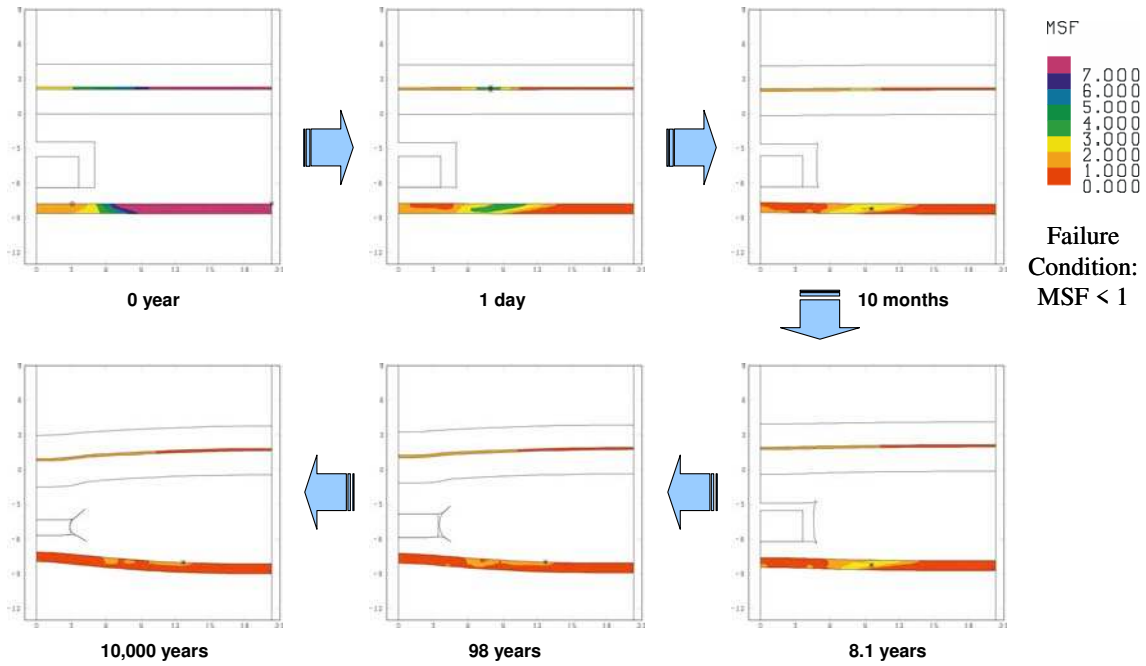
Figure 41: Changes of the shear failure zone with time in the upper and the lower anhydrite layers of the present disposal room, f=0.0.
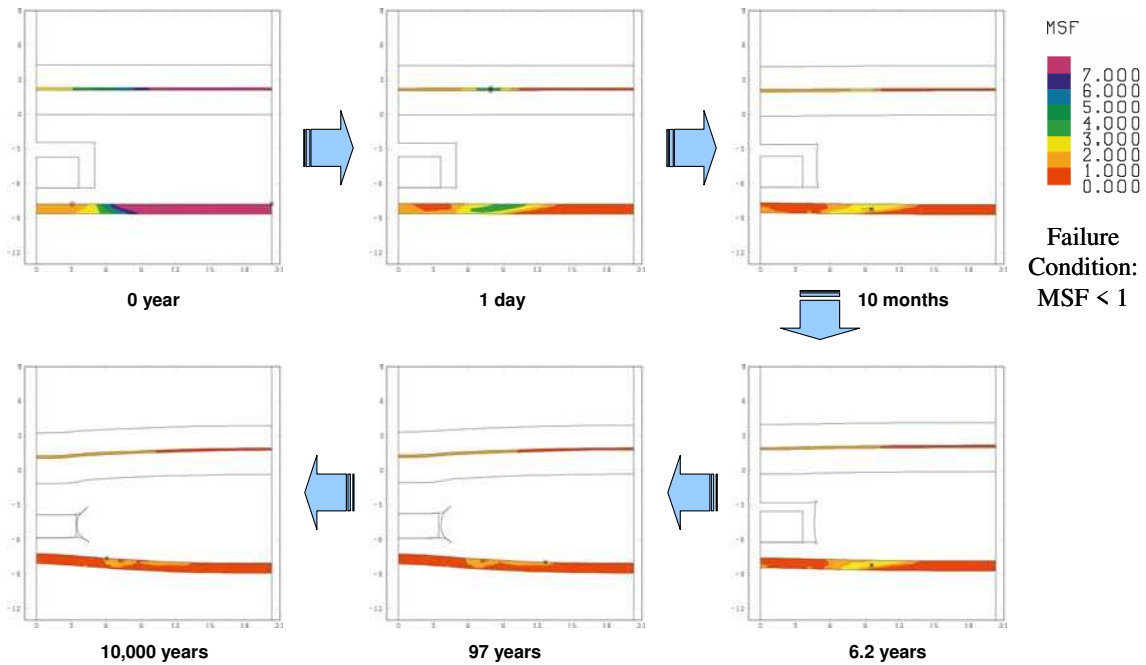
Figure 42: Changes of the shear failure zone with time in the upper and the lower anhydrite layers of the present disposal room, f=0.4.
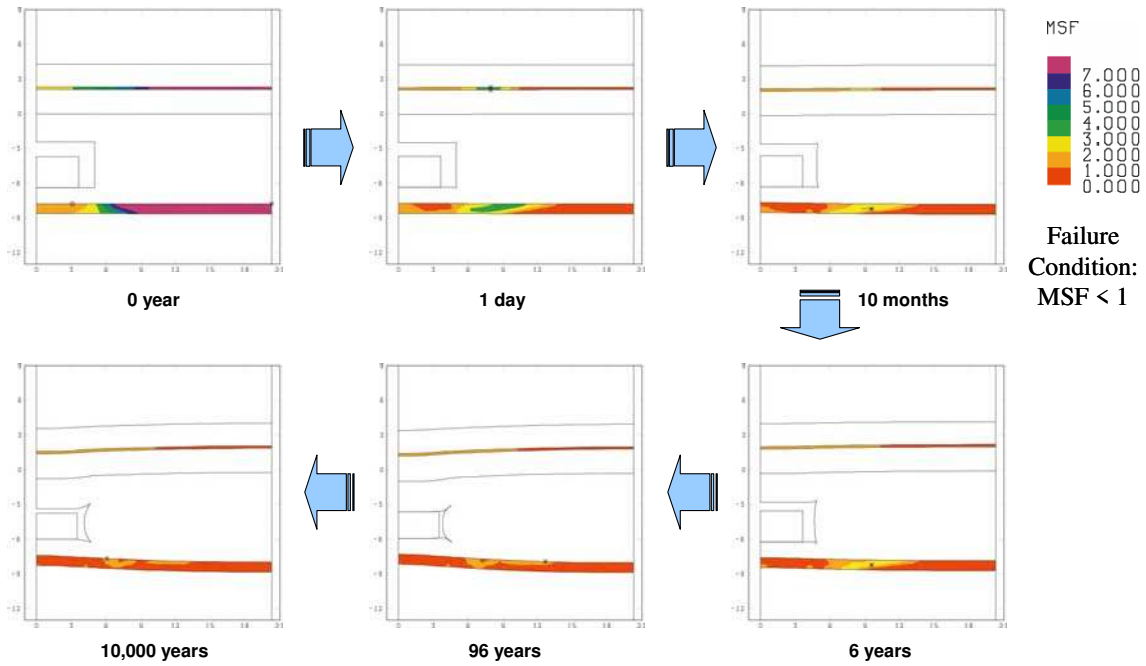
Figure 43: Changes of the shear failure zone with time in the upper and the lower anhydrite layers of the present disposal room, f=1.0.
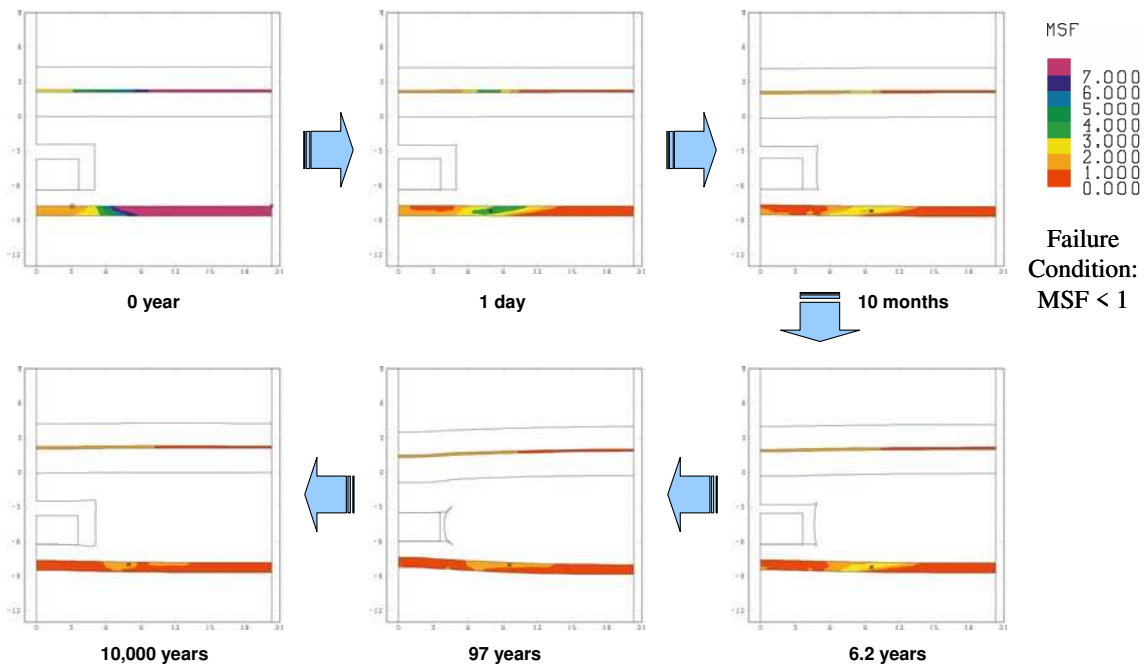
Figure 44: Changes of the shear failure zone with time in the upper and the lower anhydrite layers of the present disposal room, f=2.0.

7.6 Effect of the Input Error Found in the Original Input Data

The calculation sheet to get the SANTOS input parameters using the data in Section 2.1 and 2.2 is provided in Appendix A-3. By comparing Appendix A-3 and Appendix E, input errors were found in Stone's original input data. In the case of the waste, the density was 752 kg/m^3 in the Stone's input while the actual density is 559.5 kg/m^3 in Section 2.1.1. Two Mu was 3.333E8 Pa in Stone's input while the Two Mu of Appendix A-3 is 6.666E8 Pa. To identify the differences between the results using Stone's data and the corrected density and Two Mu data, analyses using the correct data were carried out for the gas generation factors, f = 0.0, 0.4, 1.0, and 2.0.

The porosity histories in the disposal room with time for four gas generation factors, f, are plotted as shown Figure 45. Each line indicates the results using Stone's erroneous data, and each symbol indicates the results using the corrected data. Two results coincide well with each other, which means these input errors have no effect on the results.
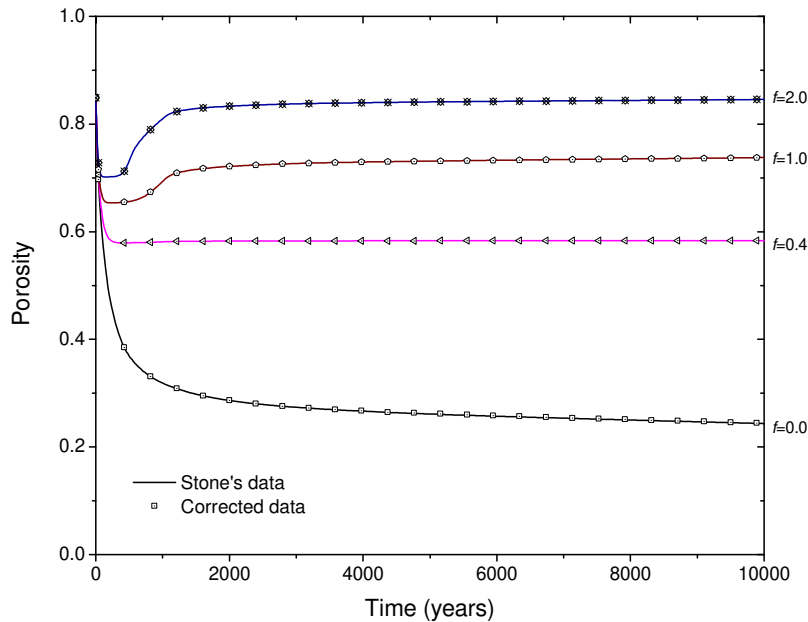
Figure 45: Porosity histories for comparing the results using Stone's data and the corrected data: Solid lines are for Stone's data and symbols are for the corrected data

63

8   SUMMARY AND CONCLUSIONS

This report summarizes a series of structural calculations executed to examine possible effects of raising the WIPP repository horizon from the original design level upward 2.43 meters. These calculations allow evaluations to be made of various features involved with the conceptual models implemented in WIPP performance assessment. Notably this work addresses issues raised in an EPA letter to Carlsbad Field Office dated August 6, 2002. In the subject letter, the EPA stated "*The conceptual model for the repository should reflect the change to raise the level of excavation to clay seam G. The conceptual change should be appropriately addressed in the modeling, if warranted*". The models implemented for Salado flow analyses including Option D have been advanced through peer review (Caporuscio, et al., 2003). The calculations in this report support the modeling concepts used for the disposal area rock mechanics. In addition, details of the geomechanical structural elements as modeled here, and provide examples of appropriate treatment of these features in performance assessment.

These calculations demonstrate that changing the repository horizon upward 2.43 m has no appreciable effect on the response of the underground relative to the computations made for the CCA. This conclusion is drawn by first comparing new results with the previous results that underpinned the compliance application. The calculation procedures and input parameters were consistent with SAND97-0795 (Stone, 1997a). These analyses used the same code, SANTOS, that supported the compliance calculations. A new validation and qualification of the software and hardware was assembled, as required by Quality Assurance procedures. Analyses using SANTOS, version 2.1.7 were carried out to a simulation time of 10,000 years, including thirteen gas generation cases. The results will be discussed in terms of four primary areas: Quality Assurance, Performance Assessment, Disturbed Rock Zone and Anhydrite Fracture.

Quality Assurance   The calculation software and platform were tested. The test cases of functionality produced essentially identical results between SANTOS version 2.1.7 and version 2.0.0. The previous results obtained by Stone (1997a) were replicated with the new SANTOS version. SANTOS version 2.1.7 was qualified as meeting requirements of the Nuclear Waste Management Procedure (NWMP) Quality Assurance Program Document (QAPD) software requirements of NP 19-1.

Performance Assessment   The hand-off to PA from the structural (finite element) calculations takes the form of a porosity surface. The models include geomechanical response of the Salado stratigraphy, the waste material, and gas generation in the disposal rooms. The volume change of the disposal room due to the salt creep is strongly dependent on the gas generation factor, *f*. The calculations used in the CCA were replicated and then repeated for grid changes appropriate for the new horizon at Clay Seam G. The gas pressure histories and porosity histories show minute differences that can be attributed to raising the disposal room. All differences between the two resultant porosity surfaces are less than 5%. This degree of comparison is believed to be well within the bounds of uncertainty and accuracy typically experienced with structural finite element models. Because the CCA porosity surface calculated for the original horizon and the new porosity

surface calculated for the raised rooms are essentially identical, no changes to the porosity surface are necessary to account for raising the repository horizon to Clay Seam G.

Disturbed Rock Zone   Calculations of the DRZ illustrate several interesting features. First the propagation of the DRZ into the surrounding rock salt does not penetrate through MB 139 in the case of both the original horizon and the raised room. The most extensive DRZ occurs at early time, say in the first ten years after the opening is mined. The DRZ above the room disappears within a short period after the ceiling of room contacts the waste.

- In the case of the raised room, the maximum extent of DRZ reaches approximately 3.8 m, the distance to the anhydrite layer (Marker Bed 139), below the room, while approximately 2.5 m over the roof of the room.

- In the case of the original horizon, the maximum thickness of upper DRZ is approximately 3.6 m over the roof of the room, while the thickness of the DRZ in the floor is 1.4 m.

- In all models the DRZ grows until the creeping salt either impinges on the waste or internal gas pressure tends to reduce the stress difference. Thereafter, the stresses trend back toward lithostatic and the DRZ criterion suggests that the DRZ is eliminated due to rock salt healing.

Based on these modeling results, some uncertainty remains with respect to healing of the DRZ. If gas production in the room provides the counterbalancing back stress, rather than the mechanical back stress provided by the waste stack, it may be that the DRZ would not heal as it would be permeated by the gas.

Anhydrite Fracture   The shear failure does not occur in either the upper or lower anhydrite layers at the moment of excavation, but appears above and below the middle of the pillar one day after the excavation. The shear stress in the anhydrite increases with time, the extent of the failure zone also increases. The internal gas pressure of the room does not affect characteristics of the shear failure zone in the anhydrite layer. The failure pattern of the present room is similar to the one of the raised room except the shear stresses in the anhydrite for the present room increase faster than the raised room. The damaged anhydrite is not expected to heal as the salt in the DRZ is expected to.

9 REFERENCES

Arguello, J. G. and Holland, J. F., 1996, *SANTOS – Verification and Qualification Document*, Carlsbad, NM: Sandia National Laboratories, Sandia WIPP Central Files WPO# 35675.

Blacker, T.D., 1988, *FASTQ Users Manual, Version 2.1*, SAND88-1326, Sandia National Labora-tories, Albuquerque, NM, July 1988.

Butcher, B.M. 1997, *A Summary of the Sources of Input Parameter Values for the WIPP Final Porosity Surface Calculations*, SAND97-0796, Albuquerque, NM: Sandia National Laboratories.

Butcher, M.M., and Mendenhall, F.T., 1993, *Summary of the Models Used for the Mechanical Response of Disposal Rooms in the Waste Isolation Pilot Plant with Regard to Compliance with 40 CFR Part 191, Subpart B*, SAND92-2347, Albuquerque, NM, Sandia National Laboratories.

Caporuscio, F., J. Gibbons, C. Li, and Oswald, E., 2003, *Salado Flow Conceptual Models Final Peer Review Report*, US Department of Energy, Carlsbad Field Office.

DOE, 2000, Letter from Dr. Triay to Mr. Marcinowski dated June 26, 2000.

EPA, 2000, Letter from Mr. Marcinowski to Dr. Triay dated August 11, 2000.

EPA, 2002, Letter from Frank Marcinowski, EPA, to Ines Triay, Carlsbad Field Office dated August 6, 2002.

Fung, Y.C., 1965, *Foundations of Solid Mechanics*, Englewood Cliffs: NJ. Prentice Hall Inc.

Gilkey, A.P. and Glick, J. H., 1991, *BLOT – A Mesh and Curve Plot Program for the Output of a Finite Element Analysis*, SAND88-1432, Sandia National Laboratories, Albuquerque, New Mexico.

Munson, D.E., and Dawson, P.R., 1979. *Constitutive Model for the Low Temperature Creep of Salt (with Application to WIPP)*, SAND79-1853, Albuquerque, NM: Sandia National Laboratories.

Munson, D.E., and Dawson, P.R., 1982, *A Transient Creep Model for Salt during Stress Loading and Unloading,* SAND82-0962. Albuquerque, NM: Sandia National Laboratories.

Munson, D.E., and Dawson, P.R., 1984. *Salt Constitutive Modeling Using Mechanism Maps*, The Mechanical Behavior of Salt, Proceedings of the First Conference, Pennsylvania State University, University Park, PA, November 9-11, 1981. Eds. H.R. Hardy, Jr. and M. Langer. Rockport, MA: Karl Distributors, 717-737.

Munson D.E. and DeVries K.L., 1991, *Development and Validation of a Predictive Technology for Creep Closure of Underground Rooms in Salt*, Proceedings: 7th International Congress on Rock Mechanics, Aachen, Germany, September 12-16.

Munson, D.E., Fossum, A.F., and Senseny, P.E., 1989, *Advances in Resolution of Discrepancies between Predicted and Measured, In Situ Room Closures*, SAND88-2948, Albuquerque, NM: Sandia National Laboratories.

Park, B.Y., 2002, *Analysis Plan for the Structural Evaluation of WIPP Disposal Room raised to Clay Seam G*, AP-093, Revision 1, Sandia National Laboratories, Carlsbad, NM.

Park, B.Y. and J.F. Holland, 2004, *Analysis Report for Structural Evaluation of WIPP Disposal Room Raised to Clay Seam G*. SAND2003-3409. Albuquerque, NM: Sandia National Laboratories.

Park, B.Y. and J.F. Holland, 2006, *Error in DRZ calculation in the Clay Seam G analysis*, Memorandum to M.Y. Lee, Sandia National Laboratories, dated December 21, 2006., WIPP:1.4.1.2:PUB:QA-L:PKG#531531.

Park, B.Y. and T.B. Kirchner, 2005, *PA Run Control Summary for Porosity Surface Calculations of the Disposal Room using SANTOS*, ERMS# 536847, Sandia National Laboratories, Carlsbad, NM.

Ratigan, J.L., Van Sambeek, L.L., 1991, *The Influence of Seal Design on the Development of the Disturbed Rock Zone in the WIPP Alcove Seal Tests*, Topical Report RSI-0400, prepared by Parsons Brinckerhoff, San Francisco, CA, and RE/SPEC Inc., Rapid City, SD, for Sandia National Laboratories, Albuquerque, NM.

Sandia National Laboratories, 1992, *Preliminary Performance Assessment for the Waste Isolation Pilot Plant, December 1992. Volume 3: Model Parameters*, SAND92-0700/3. Albuquerque, NM: Sandia National Laboratories.

Sjaardema, G.D., 1989, *NUMBERS: A Collection of Utilities for Pre- and Post-processing Two-and Three-Dimensional EXODUS Finite Element Models*, SAND88-0737, Sandia National Laboratories, Albuquerque, New Mexico.

Stone, C.M., 1996, *Proposed Model for the Final Porosity Surface Calculations*, Memorandum to B.M. Butcher, Sandia National Laboratories, Albuquerque, New Mexico, June 6, 1996.

Stone, C.M., 1997a, *Final Disposal Room Structural Response Calculations,* SAND97-0795, Sandia National Laboratories, Albuquerque, NM.

Stone, C.M., 1997b, *SANTOS-A Two-Dimensional Finite Element Program for the Quasistatic, Large Deormation, Inelastic Response of Solids*, SAND90-0543, Sandia National Laboratories, Albuquerque, NM.

Van Sambeek, L.L., Ratigan, J.L., Hansen, F.D., 1993, *Dilatancy of Rock Salt in Laboratory Tests*, Int. J. Rock Mech. Min. Sci. & Geomech. Abstr. Vol.30, No. 7, pp. 735-738.

WIPP PA (Performance Assessment), 2003, *Verification and Validation Plan/Validation Document for SANTOS 2.1.7.* , Carlsbad, NM: Sandia National Laboratories, Sandia WIPP Central Files ERMS # 530091.

Intentionally Blank

APPENDIX A: CALCULATION SHEET

A-1 Porosity
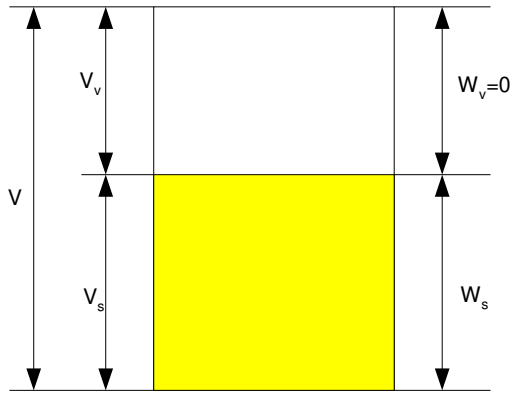
$$\rho_s = \frac{W_s}{V_s}$$

$$\rho_0 = \frac{W_s + W_v}{V} \qquad V = \frac{W_s + W_v}{\rho_0}$$

$$V_v = V - V_s = \frac{W_s + W_v}{\rho_0} - \frac{W_s}{\rho_s} = \frac{W_s}{\rho_0} - \frac{W_s}{\rho_s}$$

$$\phi = \frac{V_v}{V} = \frac{\left(\dfrac{W_s}{\rho_0} - \dfrac{W_s}{\rho_s}\right)}{\left(\dfrac{W_s + W_v}{\rho_0}\right)} = \frac{\dfrac{W_s \cdot \rho_s - W_s \cdot \rho_0}{\rho_0 \cdot \rho_s}}{\dfrac{W_s}{\rho_0}} = 1 - \frac{\rho_0}{\rho_s}$$

In the diagram: V_v, V, V_s (left labels); $W_v = 0$, W_s (right labels).

69

A-2 Initial Porosity of a Disposal Room

Height of Disposal Room: $\qquad$ $H_R := 3.96 \cdot m$

Wide of Disposal Room: $\qquad$ $W_R := 10.06 \cdot m$

Length of Disposal Room: $\qquad$ $L_R := 91.44 \cdot m$

Initial Room Volume: $\qquad$ $V_{R.i} := H_R \cdot W_R \cdot L_R \qquad V_{R.i} = 3642.8\,m^3$

Number of Drums in a Disposal Room: $\qquad$ $N_{D.R} := 6804$

Number of Drums in a Pack: $\qquad$ $N_{D.P} := 7$

Number of Packs in a Disposal Room: $\qquad$ $N_{P.R} := \dfrac{N_{D.R}}{N_{D.P}} \qquad N_{P.R} = 972$

Volume of 55-gal Steel Drums filled with Waste (SAND92-0700/3 p.3-10): $\quad V_D := 0.2539 \cdot m^3$

Volume of the All Drums filled with Waste in a Room: $\qquad$ $V_{D.W} := V_D \cdot N_{D.R} \qquad V_{D.W} = 1727.5\,m^3$

Initial Density of the All of Drums filled with Waste: $\qquad$ $\rho_0 := 559.5 \cdot \dfrac{kgf}{m^3}$

Solid Waste Density: $\qquad$ $\rho_s := 1757 \cdot \dfrac{kgf}{m^3}$

Initial Porosity of the All of Drums with Waste: $\qquad$ $\phi_0 := 1 - \dfrac{\rho_0}{\rho_s} \qquad \phi_0 = 0.682$

Initial Void Volume of the All of Drums with Waste:

$$V_{v.D.W} := V_{D.W} \cdot \phi_0 \qquad V_{v.D.W} = 1177.4\,m^3$$

Initial Solid Waste Volume: $\qquad$ $V_s := V_{D.W} - V_{v.D.W}$

$$V_s = 550.117\,m^3$$

Initial Porosity of the Undeformed Disposal Room:

$$\phi_{R.i} := \dfrac{V_{R.i} - V_s}{V_{R.i}} \qquad \phi_{R.i} = 0.849$$

A-3 Calculating the SANTOS input parameters

Halite Constitutive Model:

Shear Modulus:
$$\mu := 12400\,\text{MPa}$$
(SAND97-0796, Table 3, p.12)

Young's Modulus:
$$E := 31000\,\text{MPa}$$
(SAND97-0796, Table 3, p.12)

Poisson's ratio:
$$\nu := 0.25$$
(SAND97-0796, Table 3, p.12)

TWO MU:
$$\text{TwoMu} := 2 \cdot \mu$$

$$\text{TwoMu} = 2.48 \times 10^{10}\,\text{Pa}$$

Bulk Modulus:
$$K := \frac{E}{3 \cdot (1 - 2 \cdot \nu)}$$

$$K = 2.0667 \times 10^{10}\,\text{Pa}$$

Creep Constant:

Universal Gas Constant:
$$R := 8.3144\,10^{7} \cdot \frac{\text{erg}}{\text{mol} \cdot \text{K}}$$

Temperature:
$$T := 300\,\text{K}$$

$$Q_1 := 25000\,\frac{\text{cal}}{\text{mol}}$$
(SAND97-0796, Table 3, p.13)

$$\frac{Q_1}{R \cdot T} = 41.9633$$

$$Q_2 := 10000\,\frac{\text{cal}}{\text{mol}}$$
(SAND97-0796, Table 3, p.13)

$$\frac{Q_2}{R \cdot T} = 16.7853$$

$$c := 9.198\,10^{-3} \cdot \frac{1}{\text{K}}$$
(SAND97-0796, Table 3, p.14)

$$C := c \cdot T \qquad C = 2.7594$$

Exponent of workhardening and recovery term used to compute F: $\text{RN3} := 2.0$

Scalar multiplier of time step needed for stability, default 0.98): $\text{AMULT} := 0.95$
(SAND90-0543, p.70)

Anhydrite Constitutive Model:

Shear Modulus: $\mu := 27815\,MPa$ (SAND97-0796, Table 2.2, p.A-98)

Young's Modulus: $E := 75100\,MPa$ (SAND97-0796, Table 2.2, p.A-98)

Poisson's ratio: $\nu := 0.35$ (SAND97-0796, Table 2.2, p.A-98)

TWO MU: $TwoMu := 2 \cdot \mu$ $TwoMu = 5.563 \times 10^{10}\,Pa$

Bulk Modulus: $K := \dfrac{E}{3 \cdot (1 - 2 \cdot \nu)}$ $K = 8.3444 \times 10^{10}\,Pa$

Elastic Constant: $C := 1.35\,MPa$ (SAND97-0796, Table 1, p.B-9)

Drucker-Prager Constant: $a := 0.45$ (SAND97-0796, Table 1, p.B-9)

SANTOS Input Constant: $A0 := \sqrt{3} \cdot C$ $A0 = 2.3383 \times 10^{6}\,Pa$

$A1 := 3\sqrt{3} \cdot a$ $A1 = 2.3383$

$A2 := 0.0$ (SAND97-0796, Table 2, p.B-10)

Waste Constitutive Model:

Shear Modulus: $\mu := 333\,MPa$ (SAND97-0796, Table 7, p.18)

TWO MU: $TwoMu := 2 \cdot \mu$ $TwoMu = 6.66 \times 10^{8}\,Pa$

Bulk Modulus: $K := 222\,MPa$ $K = 2.22 \times 10^{8}\,Pa$

SANTOS Input Constant: $A0 := 1.0\,MPa$ $A0 = 1 \times 10^{6}\,Pa$

$A1 := 3.0$ $A1 = 3$

$A2 := 0.0$ (SAND97-0796, Table 7, p.18, B-9)

A-4 Modified Width and Length of the Waste

Norminal uncompressed width of the stored waste in the disposal room:

$$W_0 := 8.6\,m$$

Nominal length of the disposal room available for storing waste:

$$L_0 := 89.1 \cdot m$$

Height of the three stacked waste containers:

$$H_0 := 2.676\,m$$

Guess $\quad D := 1 \cdot m$

Given

$$(W_0 - 2 \cdot D) \cdot (L_0 - 2 \cdot D) \cdot H_0 = 1728\,m^3$$

$$D := Find(D)$$

Amount of space that must be eliminated between the drums:

$$D = 0.625 m$$

$$W := W_0 - 2D$$

Modified width of the waste:

$$W = 7.35 m$$

$$L := L_0 - 2 \cdot D$$

Modified length of the disposal room available for storing waste:

$$L = 87.85 m$$

A-5 Maximum and Minimum Gas Generation Factor

Gas produdtion potential from anoxic corrosion: $\quad p_c := 1050 \cdot \dfrac{mole}{drum}$

Gas production potential from microbial activity: $\quad p_m := 550 \cdot \dfrac{mole}{drum}$

Total gas production potential: $\quad p_t := p_c + p_m \qquad p_t = 1600 \dfrac{mole}{drum}$

from TBM analysis results for the disturbed scenario, S3

      Total moles of gas produced: $\quad m_{min} := 92032300 \, mole$

$$m_{max} := 1337650000 \, mole$$

Number of durms in WIPP: $\quad N_d := 844060 \, drum$

Minimum gas generation factor: $\quad f_{min} := \dfrac{\left(\dfrac{m_{min}}{N_d}\right)}{p_t} \qquad f_{min} = 0.07$

Maximum gas generation factor: $\quad f_{max} := \dfrac{\left(\dfrac{m_{max}}{N_d}\right)}{p_t} \qquad f_{max} = 0.99$

APPENDIX B: ALGEBRA FILE TO CALCULATE THE DRZ REGION AND THE SHEAR FAILURE REGION

```
SAVE NODAL
$
$ CONVERT STRESSES FROM PASCALS (Pa) TO MEGA-PASCALS (MPa)
$
SIGXX = SIGXX/1.0E+06
SIGYY = SIGYY/1.0E+06
SIGZZ = SIGZZ/1.0E+06
TAUXY = TAUXY/1.0E+06
VONMISES = VONMISES/1.0E+06
$
$ Compute Maximum and Minimum Principal Stresses
$
SMAX = PMAX2(SIGXX,SIGYY,TAUXY)
SMIN = PMIN2(SIGXX,SIGYY,TAUXY)
$
$ Compute mean pressure and limit it to 1.e-06
$
PRES = -( SIGXX + SIGYY + SIGZZ )/3.0
PRE = ABS(PRES) - 1.E-6
PRE2 = IFGZ(PRE,PRE,1.0E-6)
$
$ compute damage potential in the halite
$
BLOCKS 1 3
DPOT = (VONMISES/sqrt(3.0))/(3.*ABS(PRE2))
MDPOT = ENVMAX(DPOT)
$
$ compute drucker prager failure in the anhydirite
$
BLOCKS 2
PRE3 = IFEZ(PRE,1.0E-6,PRE)
SF1 = 0.45*PRE3*3. + 1.35
$
$ assume no tensile strength in the anhydrite
$
SF2 = IFGZ(SMAX,0.,SF1)
SF3 = IFLZ(SF2,0.,SF2)
$
SF = ABS(SF3)/(VONMISES/sqrt(3.0))
MSF = ENVMIN(SF)
$
$ Define time in terms of years
$
TIME = TIME/3.1536E7
$
$ Delete uneeded variables
$
DELETE PRE, PRE2, PRE3, pres,SF1,SF2,SF3
alltimes
end
```

APPENDIX C: AWK SCRIPT TO CALCULATE THE POROSITY CHANGE IN THE ROOM WITH TIME

```
#
# This awk script computes the porosity change in the room an outputs
# it as a function of time (Based upon SANTOS output)
#
BEGIN {
  dens_ws = 1757.
  dens_w  = 559.5
  vol_room = 3644.
  vol_waste = 1728.
  mass_ws = dens_w*vol_waste
  dens_room = mass_ws/vol_room
  ratio = dens_room/dens_ws
}
{
  if ( $1 ~/[0-9]/ ) {
    vol_ratio = 19.92/$2
    poro = 1. - ratio*vol_ratio
    print $1,poro
  }
}
```

APPENDIX D: FASTQ INPUT FILE

```
TITLE
 DISPOSAL ROOM MODEL - Modified by B.Y.Park (10/03/02)
POINT     1     0.00    -54.19
POINT     2    20.27    -54.19
POINT     3     0.00     -8.63
POINT     4    20.27     -8.63
POINT     5     0.00     -8.63
POINT     6    20.27     -8.63
POINT     7     0.00     -7.77
POINT     8    20.27     -7.77
POINT     9     0.00     -3.96
POINT    10     5.03     -3.96
POINT    11     0.00     -3.96
POINT    12     3.675    -3.96
POINT    13     0.00     -1.28
POINT    14     3.675    -1.28
$POINT   15     5.03     -0.00
$POINT   16     0.00     -0.00
POINT    17     0.00      0.00
POINT    18    20.27      0.00
POINT    19     0.00      4.27
POINT    20    20.27      4.27
POINT    21     0.00     52.87
POINT    22    20.27     52.87
$POINT   23    20.27     -0.00
POINT    24    20.27     -3.96
POINT    25     5.03      0.00
POINT    26     5.03     -7.77
POINT    27     5.03      4.27
POINT    28     5.03     -8.63
POINT    29     0.0       2.10
POINT    30     5.03      2.10
POINT    31    20.27      2.10
POINT    32     0.0       2.31
POINT    33     5.03      2.31
POINT    34    20.27      2.31
LINE      1    STR     1     2     0    22   1.0
LINE      2    STR     1     5     0    20   0.85
LINE      3    STR     2     6     0    20   0.85
$LINE     4    STR     5     6     0    15
LINE      5    STR    28     6     0    15   1.1
LINE      6    STR     5     7     0     4
LINE      7    STR     6     8     0     4
LINE      8    STR     7     9     0    12
LINE      9    STR    26     8     0    15   1.1
LINE     10    STR    24     8     0    12
LINE     11    STR    10    24     0    15   1.1
LINE     12    STR     9    10     0     7   0.8
LINE     13    STR    11    12     0    10
LINE     14    STR    12    14     0     7
LINE     15    STR    13    14     0    10
LINE     16    STR    11    13     0     7
LINE     17    STR    10    25     0    12
LINE     18    STR    24    18     0    12
LINE     19    STR     8    18     0    12
$LINE    20    STR    16    17     0     0
$LINE    21    STR    16    15     0     7   0.8
$LINE    22    STR    15    23     0    15   1.1
$LINE    23    STR    18    23     0     0
```

```
LINE     24      STR     25   18    0    15   1.1
LINE     25      STR     17   19    0     8
LINE     26      STR     18   20    0     8
LINE     27      STR     27   20    0    15   1.1
$LINE    28      STR     25   20    0     8
LINE     29      STR     19   21    0    20   1.15
LINE     30      STR     20   22    0    20   1.15
LINE     31      STR     21   22    0    22   1.0
LINE     32      STR     17   25    0     7   0.8
LINE     33      STR     19   27    0     7   0.8
LINE     34      STR      7   26    0     7   0.8
LINE     35      STR      5   28    0     7   0.8
LINE     36      STR     17   29    0     4
LINE     37      STR     18   31    0     4
LINE     38      STR     29   30    0     7   0.8
LINE     39      STR     30   31    0    15   1.1
LINE     40      STR     29   32    0     1
LINE     41      STR     31   34    0     1
LINE     42      STR     32   33    0     7   0.8
LINE     43      STR     33   34    0    15   1.1
LINE     44      STR     32   19    0     4
LINE     45      STR     34   20    0     4
SIDE    100      11   12
$SIDE   101      21   22
SIDE    102      32   24
SIDE    103      33   27
SIDE    104      35    5
SIDE    105      34    9
SIDE    106      38   39
SIDE    107      42   43
$ NODEBC CARDS
NODEBC   2    1
NODEBC   1    2     6    8    16    36    40    44    29
NODEBC   1    3     7   10    18    37    41    45    30
$ SIDEBC CARDS
SIDEBC  10   31
SIDEBC  20    1    $ added
SIDEBC 100   12
SIDEBC 200   17
SIDEBC 300   32
SIDEBC 400   13
SIDEBC 500   14
SIDEBC 600   15
SIDEBC 700   12   17    32
$ REGION CARDS
REGION   1    1   -1   -3   104   -2
REGION   2    2  104   -7   105   -6
REGION   3    1  105  -10   100   -8
REGION   4    1  -11  -18   -24  -17
$REGION   5    1  101  -23   102  -20
REGION   6    3  102  -37   106  -36
REGION   7    1  103  -30   -31  -29
REGION   8    4  -13  -14   -15  -16
REGION   9    2  106  -41   107  -40
REGION  10    3  107  -45   103  -44
SCHEME   P
EXIT
```

APPENDIX E: SAMPLE SANTOS INPUT FILE FOR CLAY SEAM G ANALYSIS

```
TITLE
Structural Response of Disposal Rooms Raised 2.43 m (Gas Factor: f=0.1)
PLANE STRAIN
INITIAL STRESS = USER
GRAVITY = 1 = 0. = -9.79 = 0.
PLOT ELEMENT, STRESS, STRAIN, VONMISES, PRESSURE
PLOT NODAL, DISPLACEMENT, RESIDUAL
PLOT STATE, EQCS, EV
RESIDUAL TOLERANCE = 0.5
MAXIMUM ITERATIONS = 1000
MAXIMUM TOLERANCE = 100.
INTERMEDIATE PRINT = 100
ELASTIC SOLUTION
PREDICTOR SCALE FACTOR = 3
AUTO STEP .015 2.592E6 NOREDUCE 1.E-5
TIME STEP SCALE = 0.5
HOURGLASS STIFFENING = .005
STEP CONTROL
500 3.1536e7
2000 3.1536e9
36000 3.1536e11
END
OUTPUT TIME
1 3.1536e7
1 3.1536e9
200 3.1536e11
END
PLOT TIME
10 3.1536e7
100 3.1536e9
120 3.1536e11
END
MATERIAL, 1, M-D CREEP MODEL, 2300. $ ARGILLACEOUS HALITE
TWO MU = 24.8E9
BULK MODULUS = 20.66E9
A1 = 1.407E23
Q1/R = 41.94
N1 = 5.5
B1 = 8.998E6
A2 = 1.314E13
Q2/R = 16.776
N2 = 5.0
B2 = 4.289E-2
SIG0 = 20.57E6
QLC = 5335.
M = 3.0
K0 = 2.47E6
C = 2.759
ALPHA = -14.96
BETA = -7.738
DELTLC = .58
RN3 = 2.
AMULT = .95
END
MATERIAL, 2, SOIL N FOAMS, 2300. $ ANHYDRITE
TWO MU = 5.563E10
BULK MODULUS = 8.3444E10
A0 = 2.338e6
A1 = 2.338
A2 = 0.
PRESSURE CUTOFF = 0.0
FUNCTION ID = 0
END
```

```
MATERIAL, 3, M-D CREEP MODEL, 2300. $ PURE HALITE
TWO MU = 24.8E9
BULK MODULUS = 20.66E9
A1 = 8.386E22
Q1/R = 41.94
N1 = 5.5
B1 = 6.086E6
A2 = 9.672E12
Q2/R = 16.776
N2 = 5.0
B2 = 3.034E-2
SIG0 = 20.57E6
QLC = 5335.
M = 3.0
K0 = 6.275E5
C = 2.759
ALPHA = -17.37
BETA = -7.738
DELTLC = .58
RN3 = 2.
AMULT = .95
END
MATERIAL, 4, SOIL N FOAMS, 752.
TWO MU = 3.333E8
BULK MODULUS = 2.223E8
A0 = 1.0e6
A1 = 3.
A2 = 0.
PRESSURE CUTOFF = 0.
FUNCTION ID = 2
END
NO DISPLACEMENT X = 1
NO DISPLACEMENT Y = 2
PRESSURE, 10, 1, 13.57E6
CONTACT SURFACE, 100, 400, 0., 1.E-3, 1.E40
CONTACT SURFACE, 200, 500, 0., 1.E-3, 1.E4
CONTACT SURFACE, 300, 600, 0., 1.E-3, 1.E4
CONTACT SURFACE, 300, 200, 0., 1.E-3, 1.E4
CONTACT SURFACE, 100, 200, 0., 1.E-3, 1.E4
ADAPTIVE PRESSURE, 700, 1.e-6, -6.4
FUNCTION,1 $ FUNCTION TO DEFINE PRESCRIBED PRESSURE
0., 1.
3.1536e11, 1.
END
FUNCTION,2
0.0000, 0.0000
0.5101, 1.5300E6
0.6314, 2.0307E6
0.7189, 2.5321E6
0.7855, 3.0312E6
0.8382, 3.5301E6
0.8808, 4.0258E6
0.9422, 4.9333E6
1.1400, 12.000E6
END
FUNCTION = 3
0. 0.5
3.1536E11 1.
END
EXIT
```

APPENDIX F: SAMPLE USER SUBROUTINES

F-1 Adaptive Pressure Boundary condition

```
      SUBROUTINE FPRES( VOLUME,TIME,PGAS )
C ....
C .... THE PRESSURE IS COMPUTED ON THE BASIS OF THE IDEAL GAS LAW,
C .... PV = NRT. THE TOTAL NUMBER OF MOLES OF GAS, N (EN), PRESENT
C .... AT ANY TIME IS DETERMINED ON THE BASIS OF A CONSTANT RATE OF GAS
C .... GENERATION. R IS THE UNIVERSAL GAS CONSTANT AND THETA IS THE ROOM
C .... TEMPERATURE, 300 K. V IS THE CURRENT VOLUME OF THE ROOM. THE VOLUME
C .... MUST BE CORRECTED BY MULTIPLYING BY 2 OR 4 TO ACCOUNT FOR THE USE OF
C .... HALF OR QUARTER-SYMMETRY MODELS. THE VOLUME MUST ALSO BE MULTIPLIED
C .... BY A FACTOR TO ACCOUNT FOR 3D LENGTH.
C ....
C
      INCLUDE 'precision.blk'
C
      R = 8.314
      THETA = 300.
C
      IF( TIME .LT. 1.7325E10 )THEN
         PVALUE = 0.0
         RATE = 4.32E-4
         TSTAR = 0.0
      ELSE IF( TIME .LT. 3.3075E10 )THEN
         PVALUE = 7.48E6
         RATE = 2.16E-4
         TSTAR = 1.7325E10
      ELSE
         PVALUE = 1.0886e7
         RATE = 0.0
         TSTAR = 0.0
      END IF
C
C .... CORRECT VOLUME AT THIS TIME TO GET VOLUME OF VOIDS
C
      EN = PVALUE + RATE * ( TIME - TSTAR )
C      SCALE = 2.
      SCALE = 0.1
      SYMFAC = 2.
      XLENG = 91.44
C
C .... THIS MODIFICATION REMOVES THE BACKFILL FROM VSOLID
C
C VSOLID FOR WASTE AND DRUMS ONLY 551.2
      VSOLID = 551.2
      VOLUME = SYMFAC * VOLUME * XLENG - VSOLID
      IF( VOLUME .LE. 0.0 )VOLUME = 1.
C
      PGAS = SCALE * EN * R * THETA / VOLUME
C
      RETURN
      END
```

F-2 Initial Stress State

```
      SUBROUTINE INITST( SIG,COORD,LINK,DATMAT,KONMAT,SCREL )
C
C **********************************************************************
C
C   DESCRIPTION:
C     THIS ROUTINE PROVIDES AN INITIAL STRESS STATE TO SANTOS
C
C   FORMAL PARAMETERS:
C     SIG        REAL        ELEMENT STRESS ARRAY WHICH MUST BE RETURNED
C                            WITH THE REQUIRED STRESS VALUES
C     COORD      REAL        GLOBAL NODAL COORDINATE ARRAY
C     LINK       INTEGER     CONNECTIVITY ARRAY
C     DATMAT     REAL        MATERIAL PROPERTIES ARRAY
C     KONMAT     INTEGER     MATERIAL PROPERTIES INTEGER ARRAY
C
C   CALLED BY: INIT
C
C **********************************************************************
C
      INCLUDE 'precision.blk'
      INCLUDE 'params.blk'
      INCLUDE 'psize.blk'
      INCLUDE 'contrl.blk'
      INCLUDE 'bsize.blk'
      INCLUDE 'timer.blk'
C
      DIMENSION LINK(NELNS,NUMEL),KONMAT(10,NEMBLK),COORD(NNOD,NSPC),
     *          SIG(NSYMM,NUMEL),DATMAT(MCONS,*),SCREL(NEBLK,*)
C
      DO 1000 I = 1,NEMBLK
         MATID = KONMAT(1,I)
         MKIND = KONMAT(2,I)
         ISTRT = KONMAT(3,I)
         IEND = KONMAT(4,I)
            DO 500 J = ISTRT,IEND
               II = LINK( 1,J )
               JJ = LINK( 2,J )
               KK = LINK( 3,J )
               LL = LINK( 4,J )
               ZAVG = 0.25 * ( COORD(II,2) + COORD(JJ,2) + COORD(KK,2) +
     *               COORD(LL,2) )
               STRESS = - 2300. * 9.79 * ( 655. - ZAVG )
               IF( MATID .EQ. 4 )THEN
                  STRESS = 0.
               END IF
               SIG(1,J) = STRESS
               SIG(2,J) = STRESS
               SIG(3,J) = STRESS
               SIG(4,J) = 0.0

  500       CONTINUE
 1000 CONTINUE
      RETURN
      END
```

DISTRIBUTION

2 U.S. Department of Energy
  Attn: D. Johnson, FE-42
    D. Buck, FE-42
  Strategic Petroleum Reserve
  1000 Independence Avenue SW
  Washington, D.C. 20585

1 US Department of Energy
  Attn: Deputy Director, RW-2
  Office of Civilian Radioactive Waste Mgmt.
  Forrestal Building
  Washington, DC 20585

Electronic copy only to Wayne Elias at Elias.Wayne@spr.doe.gov for distribution to DOE and DM

1	MS0376	M. L. Staten	1421
1	MS0376	J. E. Bean	1524
1	MS0376	C. M. Stone	1525
1	MS0376	J. G. Arguello Jr.	1525
1	MS0701	P. B. Davies	6700
1	MS0701	F. B. Nimick	6790
1	MS1002	S. Roehrig	6300
1	MS0706	D. J. Borns	6312
10	MS0706	B. L. Ehgartner	6312
1	MS0706	D. L. Lord	6312
1	MS0706	D. E. Munson	6312
1	MS0706	C. C. Rautman	6312
1	MS0706	A. R. Sattler	6312
1	MS0706	A. C. Snider Load	6312
1	MS0735	J. A. Merson	6310
1	MS0735	R. E. Finley	6313
1	MS0754	T. E. Hinkebein	6316
1	MS0751	L. S. Costin	6315
1	MS0751	T. W. Pfeifle	6311
1	MS0751	S. R. Sobolik	6315
1	MS0776	M. K. Knowles	6781
1	MS0776	J. S. Stein	6782
1	MS0778	F. D. Hansen	6785
1	MS1031	D. R. Bronowski	6315
1	MS1104	M. L. Tatro	6200
1	MS1395	D. S. Kessel	6710
5	MS1395	M. Y. Lee	6711

10	MS1395	B. Y. Park	6711
1	MS1395	C. G. Herrick	6711
1	MS1395	E. D. Vugrin	6711
1	MS1395	M. J. Rigali	6712
1	MS1395	L. H. Brush	6712
2	MS9018	Central Technical Files	8944
2	MS0899	Technical Library	4536
1	MS0731	823 Library	6850
1	MS0612	Review and Approval Desk, For DOE/OSTI	9612